REVIEW

Check for updates

Electrochemical ammonia synthesis: fundamental practices and recent developments in transition metal boride, carbide and nitride-class of catalysts

Ashmita Biswas, [ID] † Sakshi Bhardwaj,† Tribani Boruah† and Ramendra Sundar Dey [ID] *

Ammonia, a value-added chemical, major fertilizer and future transportation fuel, is conventionally and synthetically produced by the energy intensive Haber−Bosch process. For the conversion of nitrogen to ammonia, more energy efficient and environmentally friendly approach is required which can be fulfilled by the electrochemical nitrogen reduction reaction (NRR). Because of its sluggish kinetics and poor selectivity, the progress of NH_3 production is far beyond the industrial periphery. So, to meet the current energy demands, here we have summarized the bottlenecks of the NRR and have discussed briefly how to over-come these issues in terms of competitive HER, N_2 solubility in the electrolyte, and material specificity. Among the various categories of catalysts explored for NRR, we are here interested in transition metal borides (Mbenes), carbides (TMCs) and nitrides (TMNs) because of their respective benefits in selective N_2 adsorption and its subsequent reduction. We have widely covered the DFT studies concerning these catalysts and their experimental implementations towards NRR. Along with that, we believe that this review with detailed funda-mentals of N_2 reduction will act as a tutorial for new-comers in this field. Finally, with the focus on the cur-rent challenges in this field, potential opportunities and future prospective have been provided.

Institute of Nano Science and Technology, Sector-81, Mohali, Punjab, India. E-mail: rsdey@inst.ac.in

† These authors contributed equally.

Ashmita Biswas received her bachelor's degree with Chemistry Honours from the University of Calcutta in the year 2017. She has completed her master's degree from Indian Institute of Engineering Science and Technology, Shibpur, India (2017–2019). She is currently pursuing her PhD under the super-vision of Dr Ramendra Sundar Dey at Institute of Nano Science and Technology, Mohali, India and Indian Institute of Science Educa-tion and Research, Mohali, India.

Ashmita Biswas

She has published five research papers in peer-reviewed journals and provisionally filed one patent. Her research interest includes the development of noble-metal-free catalysts applicable for electrocatalytic reduction reactions in the field of sustainable energy.

Sakshi Bhardwaj is currently a PhD candidate under the supervision of Dr Ramendra Sudar Dey in Institute of Nanoscience Science and Technology (INST), Mohali, India and Indian Institute of Science Education and Research, Mohali, India. She received her master's degree in chemistry from Guru Nanak Dev University, India, in 2018. Her current research focuses on the engineering of defect sites of carbonaceous nano-materials for electrocatalytic applications.

Sakshi Bhardwaj

1. Introduction

Ammonia (NH_3) is an important industrial chemical, useful fertilizer as well as a next generation renewable energy source for fuel cell technology.[1] But its synthesis uses up to 3 to 5% of the world's natural gas. Therefore, a lot of research is being done all over the world for the electrocatalytic NH_3 synthesis by nitrogen reduction reaction (NRR) under ambient conditions, which is a promising alternative to the famous century-old Haber–Bosch process.[2] The major obstacles to this electrochemical process are the solubility issue of N_2 in the electrolyte medium, competitive hydrogen evolution reaction (HER) occurring at the same voltage window as that of NRR, selectivity of most of the metals towards H_2 adsorption than N_2 and the sluggish counter-oxidation reaction at the anode.[3] These are indeed major concerns as these factors directly affect the yield, production rate and faradaic efficiency (F.E.) of NH_3 synthesis. A detrimental NRR kinetics makes way for the facile HER process.[4,5] Moreover, a false positive NH_3 production is often encountered if there is any nitrogenous source other than the feeding gas.[6] Thus, several precautionary measures are a must to adopt during the NRR process. This approach had been initiated in the late 1960s; however, the field has started its development recently. With an attempt to gain industrial scale NH_3 production, several new avenues got opened in the process of catalyst designing and electrolyte improvisation. While some researchers started working on membranes to capture protons and help easy diffusion of N_2, so that there is less interference of H^+ ions and restricted HER, others were more interested in investigating the reaction mechanisms being followed during NRR.

Thus, this field has enormously widened with enough room for further exploration and development.[7]

Ren *et al.* have clearly demonstrated that about 90% of the research works on NRR are concerned with catalyst designing.[4] The catalyst should be such that either it should be selective to N_2 adsorption rather than protons or it should be engineered to have HER suppression ability by blocking the HER active sites. Considering the latter, several approaches have been adopted by researchers which include defect engineering, interface engineering, phase specific material designing and induced strained effects to gain dominance of NRR over HER.[8–14] However, it is desirable to have a simpler catalyst system but with efficacy to meet the current demands for high NH_3 production with improved current density and faradaic efficiency (F.E.) because a rather complicated system would only add to the constraints of NRR.

Transition metal borides, carbides and nitrides have drawn immense attention in this field for their advantages over other classes of catalysts. Transition metal borides take the advantages of dual active edges (from the metal end as well as the boride end).[15] It is known that transition metals have σ-donation and π-back donation interactions with the adsorbed N_2.[16] However, it is noteworthy to mention that, borides can have energy as well as symmetry matched 2p orbital overlap with N_2, which favours N_2 adsorption on the B-active edges.[17] In the case of transition metal carbides, owing to the bonding interactions of 2s and 2p orbitals of the C atoms with the d orbital of the transition metals, their electronic structures resemble those of noble metals near the Fermi edge.[18] This reinforces the intrinsic electronic properties of these catalysts

Tribani Boruah is currently pursuing her PhD from the Institute of Nano Science and Technology (INST), Mohali, India, under the supervision of Dr Ramendra Sundar Dey. She received her BSc degree in chemistry from Dibrugarh University, Assam, India, in 2016 and completed her masters from University of Delhi, New Delhi, India, in Organic Chemistry in the year 2019. Her current research interest includes the synthesis of non-precious metal-based Air electrode for rechargeable metal air batteries.

Tribani Boruah

Ramendra Sundar Dey is a Scientist at Institute of Nano Science and Technology, Mohali, India. Prior, he was a Hans Christian Ørsted postdoc fellow at Technical University of Denmark (DTU), Denmark. He received his PhD in chemistry in 2013 from Indian Institute of Technology (IIT) Kharagpur, India. He is involved in research in the field of electrochemistry of nanomaterials. His research interests focus on the architecture and engineering of nanomaterials for advanced energy storage technology and non-novel metal nanomaterials for electrocatalysis and hybrid energy technology. He has been honored with a number of prestigious national and international recognitions, like INSPIRE Faculty Award for 2015, Journal of Materials Chemistry A Emerging Investigator under the theme highlighting 2019's rising stars of materials by RSC. Recently he has been awarded as the Associate of Indian Academy of Science, Bengaluru, and member of the Indian National Young Academy of Sciences (INYAS).
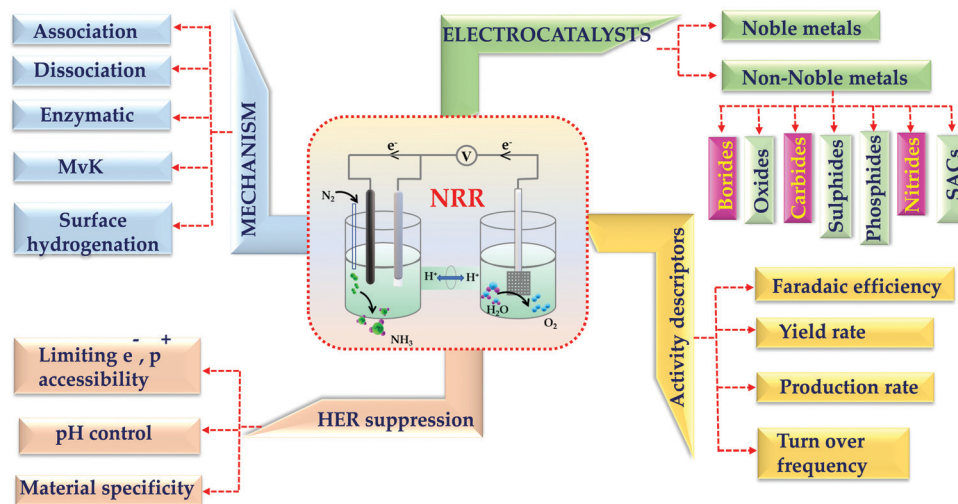
Ramendra Sundar Dey

Fig. 1   A systematic summary of electrochemical nitrogen reduction reaction.

and helps to promote electron transfer from the catalyst surface to the reactants during NRR, enabling better charge transfer rates and NRR kinetics. Different from these two classes, the transition metal nitrides have inherent N-atoms, which act as the commencer of the NRR process on these catalysts.[19] Basically, the competition of NRR with HER arises because of the competition between proton and N_2 adsorption selectivity on the catalyst surface. But in this case, because of the special mars-van Krevelen mechanism, NRR dominates over HER.[20] Considering all these key points, in this review firstly we have briefed the fundamentals of NRR followed by all the important experimental conditions like electrolytes favouring N_2 solubility in the medium, pH of the medium, proton and electron accessibility limiting HER kinetics and the choice of metals favouring NRR. Further, we have elaborated the gradual progress of the transition metal borides, carbides and nitrides for NRR and also reviewed the limitations and scopes with these classes of catalysts. Fig. 1 demonstrates the scope of this review. We believe that, this review will be helpful enough for the newcomers in this field to design transition metal borides, carbides and nitrides preferably for NRR with high yield, production rate and faradaic efficiency for NH_3 synthesis.

2. Fundamental basis of NRR

2.1 Thermodynamics of NRR

Dinitrogen (N_2) molecules are extremely inert owing to the high bond dissociation energy (941 kJ mol^{-1}) of the triple bond, which accounts for just a portion of their inertness. The greater triple bond energy (962 kJ mol^{-1}) in acetylene (C_2H_2), although C_2H_2 is significantly highly reactive than N_2, is an obvious cause for the reactivity discrepancy. The first H-atom addition to N_2 is endothermic (+37.6 kJ mol^{-1}), while the reaction with C_2H_2 is exothermic (-171 kJ mol^{-1}). Apparently direct protonation is generally allowed for C_2H_2, but not for N_2.[21] N_2 has a low electron affinity (1.9 eV) and a high ionization potential (15.8 eV). The wide energy gap (10.82 eV) between the highest

occupied (HOMO) and the lowest vacant molecular orbitals (LUMO) of N_2 discourages electron transport reactions.[22,23]

The thermodynamic limitations imposed by the reaction intermediates explain the key bottlenecks in the reduction reaction of N_2 to NH_3. The electrocatalytic reduction of N_2 to NH_3 has similar equilibrium potentials to that of the contending HER. Among aqueous electrolytes, H_2 is the primary NRR side product. Regardless, the NRR involves numerous proton–electron transfer pathways with intermediates. Although the redox potentials for the production of the N_2H intermediate are quite negative, this indicates that the initial H-atom addition is extremely challenging. When applied to multistep catalytic processes comprising various intermediates, the thermodynamic methodology has highlighted significant shortcomings. The relative adsorption energy levels of several NRR intermediates could be scaled up in terms of Gibbs' energy requirement for each step.[24] It is challenging to find an ideal catalyst with all reaction stages being thermodynamically neutral or favorable. There are no independent binding energies for the NH_2 or N_2H intermediate in NRR, resulting in a minimal overpotential of 0.4 V.[25] Fortunately, subsequent theoretical calculations have revealed potential innovative ways to decrease overpotential which may be employed to break or avoid the scaling relations of NRR.

2.2 Different mechanistic approaches

In nature, plants can reduce nitrogen through numerous proton and electron transfer processes, which are catalyzed by iron-molybdenum nitrogenase enzymes under environmental conditions.[26–28] The nitrogenase enzymes having Fe–Fe, Fe–Mo and Fe–V active moieties are believed to go through the reduction process by the enzymatic pathway where N_2 undergoes side-on adsorption on the catalyst surface followed by alternative hydrogenation of each of the N atoms. This results in the release of two NH_3 molecules subsequently. Nevertheless, analyzing and understanding the nitrogen fixation mechanism continues to be a difficult endeavor in the living organisms.

After more than 150 years of research, F. Haber was able to effectively develop an artificial nitrogen-fixing industrial process[29] in order to meet the demands of the manufacturing sector. Eqn (1) describes how an ammonium-containing combination of nitrogen and hydrogen is utilized to create ammonia under extreme conditions of high temperature and pressure while engaging a catalyst:

$$N_2 + 3H_2 = 2NH_3, \Delta H_0 = -45.9 \text{ kJ mol}^{-1} \quad (1)$$
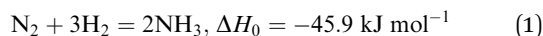
In contrast to the HER and ORR, where the reaction pathway has been well known using metal (Pt) model catalytic systems, the NRR lacks an appropriate catalyst to examine the mechanism, as standard noble metal catalysts, which work well in the HER and ORR, do not operate well in the NRR. The NRR reaction mechanism is still not clear, although the three main reaction mechanisms currently acknowledged are the dissociative mechanism, the associative pathway (alternating and distal), and the enzymatic pathway.[29,30] In the dissociative mechanism, the N–N bond is broken first and then the two N atoms are adsorbed on

to the catalyst, indicating the catalytic hydrogenation reaction, which is most prevalent in the Haber–Bosch technique because the kinetic parameters can provide enough power to impede the N≡N bond which is illustrated in Fig. 1.[26] The hydrogenation reaction is initiated before the breakdown of the N–N bond in the associative pathway.[31] Almost all the catalysts lean towards the associative mechanism of ammonia synthesis, which is further categorized into alternating and distal pathways. The alternating pathway is the same as the enzymatic pathway except for the fact that here, N_2 undergoes end-on adsorption on the catalyst surface. This end-on adsorption is possible when the catalysts have free unsaturated sites (axially) for N_2 adsorption. For the distal pathway, the farthest N atom is first protonated and released as NH_3, followed by the protonation of the next N ad-atom. Au/TiO_2[32] B-induced O vacant MnO_2[33] and the S-vacant amorphous MoS_3 catalyst[34] follow the distal associative pathway, while the N-vacant polymeric carbon nitride[35] follows an alternating associative pathway, where the two N-atoms alternately hydrogenate even before the N–N bond breaks, resulting in the
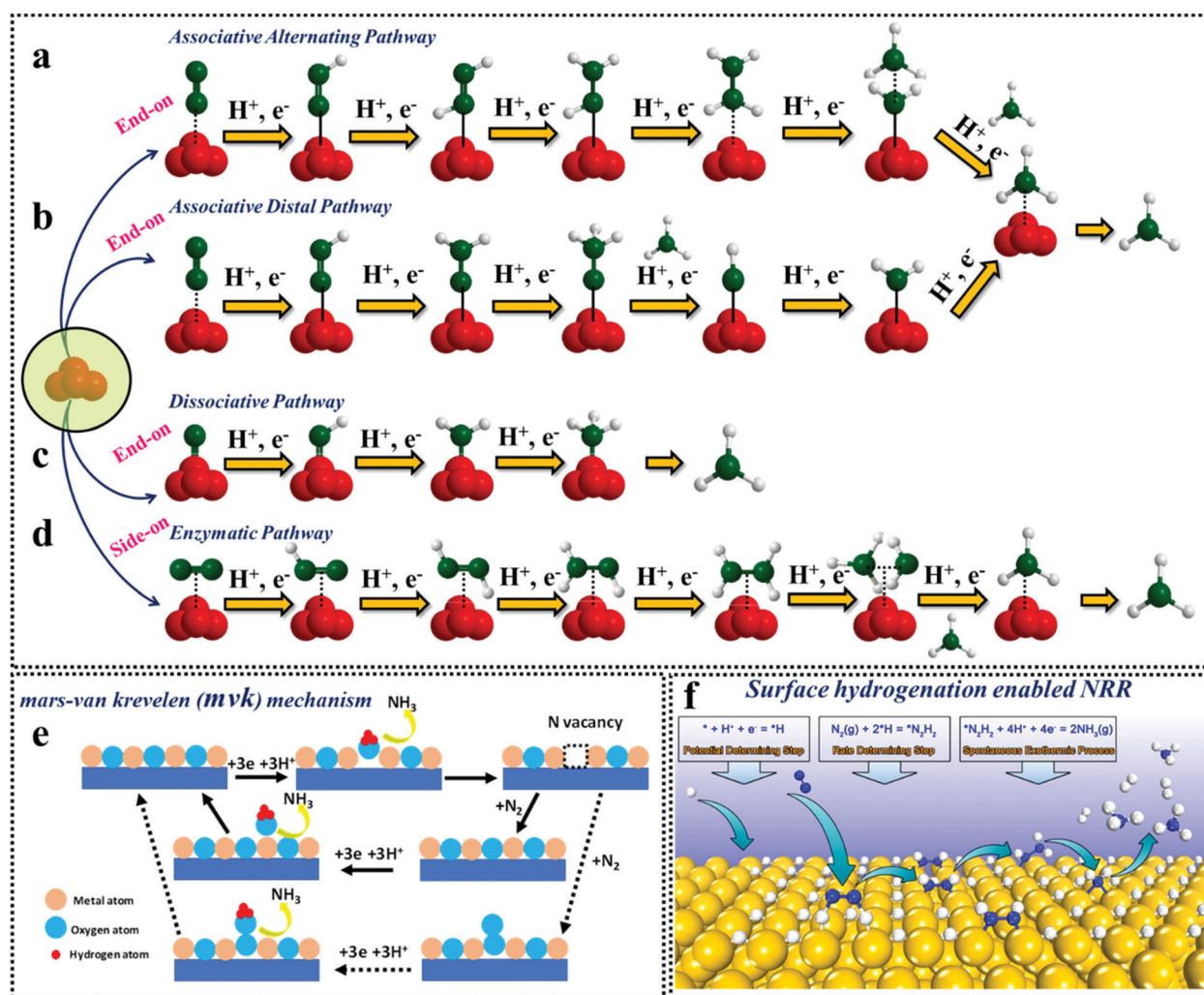

Fig. 2 Different mechanistic approaches of NRR. (a) Associative alternating pathway; (b) associative distal pathway; (c) dissociative pathway; (d) enzymatic pathway; (e) Mars–van Krevelen pathway and (f) surface hydrogenation driven NRR. Reproduced with permission from Ling *et al.*,[41] Copyright 2019, American Chemical Society.

release of one NH_3 molecule followed by another ammonia molecule. The different mechanistic approaches adopted for NRR are elaborated in Fig. 2a–d.

A special class of the N_2 reduction mechanism is the Mars-van Krevelen pathway (Fig. 2e), which is mostly prevalent for transition metal nitrides.[36] In this case, the N atom of the active element takes part in the NH_3 synthesis besides the N_2 gas purged into the electrochemical system. Although W_2N_3 is known to follow this pathway, upon creating N vacancies in W_2N_3, the reaction deviates to the distal associative pathway.[37] A recent report suggests that, even O-vacant V_2O_5 and CeO_2 are interpreted within the Mars–van Krevelen mechanism for ammonia synthesis.[38] While the class of anion vacancy inherited transition metal based electrocatalysts follow the associative pathway, a class of boron doped carbon nitride compounds tend to follow the enzymatic pathway at the cost of a low energy barrier.[39,40]

Recently, another interesting mechanistic approach has been highlighted by Ling et al., where they have focused on the weak N_2 binding on the surface of noble-metal catalysts. They suggested a surface hydrogenation triggered NRR (Fig. 2f) on these noble metal surfaces where the first step was the adsorption of H^+. Thereafter, under a relatively high coverage of *H, N_2 got activated and reduced into $*N_2H_2$ by surface *H. Subsequently, the produced $*N_2H_2$ reduced into NH_3 spontaneously. In this case, the reduction of H^+ is the potential-determining step, while the activation and reduction of N_2 into $*N_2H_2$ is the rate-determining step as shown in the figure.[41]

2.3 Activity descriptors for NRR

When it comes to electrocatalytic NRR, the production of NH_3 and the faradaic efficiency (FE) are the two most important factors to take into consideration. The yield of any chemical substance is the most important consideration. In the case of NRR, the NH_3 yield rate reflects the amount of ammonia produced per unit mass/area of catalyst loading with unit time, and it is intended to monitor the effectiveness of electrocatalysts. While conducting experimental investigations, this yield can be determined in $\mu g\ h^{-1}\ mg_{cat}^{-1}$ by using the chronoamperometry quantitative study, which is represented by eqn (2), where C is the measured NH_3 concentration ($\mu g\ mL^{-1}$), V is the volume of the electrolyte in the cathodic compartment, t is the electrolysis time, and mg_{cat} is the mass of the catalyst loaded on the cathode surface.

$$R = \frac{C \times V}{t \times mg_{cat.}} \quad (2)$$

Another measurement of the selectivity of an electrochemical process for NH_3 production in comparison to competing reactions such as HER is the fraction of faradaic current used for nitrogen reduction in relation to the total current passed through the circuit. The following equation (eqn (3)) can be used to calculate the FE, where n is the number of electrons required for producing one NH_3 molecule (n = 3), F is the Faraday constant (F = 96 485 C mol^{-1}), C is the measured NH_3 concentration ($\mu g\ mL^{-1}$), V is the volume of the electrolyte in the

cathode compartment (mL), M is the relative molar mass of NH_3 (M = 17 g mol^{-1}), and Q is the total charge passed through the electrodes (C).

$$\text{F.E.} = \frac{n \times F \times C \times V}{M \times Q} \quad (3)$$

The surface-area-normalized production rate of NH_3 (mol $s^{-1}\ cm^{-2}$) was calculated by eqn (4) as below:

$$\text{Production rate}_{ECSA} = \frac{C \times V}{M \times t \times A_{ECSA}} \quad (4)$$

where A_{ECSA} represents the electrochemically active surface area of the active material.

The mass-normalized production rate of NH_3 (mmol $h^{-1}\ g_{cat}^{-1}$) was calculated as below (eqn (5)):

$$\text{Production rate}_{mass} = \frac{C \times V}{M \times t \times g_{cat}^{-1}} \quad (5)$$

where n is the number of electrons required for producing one NH_3 molecule (n = 3), F is the Faraday constant (F = 96 485.33), M is the relative molecular mass of NH_3 (M = 17.03), and Q is the overall charge that passes via the electrodes.

Likewise, another important parameter is the turn-over frequency (TOF) of the electrocatalyst, which is a measure of the instantaneous efficiency of a catalyst, calculated as the derivative of the number of turnovers of the catalytic cycle with respect to the time per active site of the catalyst. It is given by the following equation:[42]

$$\text{TOF (h}^{-}) = \frac{r_N \times N_A/1000}{N_{sas}} \quad (6)$$

where TOF is the turnover frequency (in h^{-1}), r_N is the ammonia-producing rate (in mmol $g^{-1}\ h^{-1}$), N_A is the Avogadro constant ($6.023 \times 10^{23}\ mol^{-1}$) and N_{sas} is the number of surface sites (in g^{-1}).

3. Rate determining factors for NRR

3.1 N_2 solubility in the electrolyte

The most vital factor that is responsible for the low yield and production rate of NH_3 is the poor solubility of N_2 in the aqueous medium. Recently, Choi et al. have concluded that the catalysts that deliver low yield and production rate of NH_3 fail to be convincing enough to actually reduce the dinitrogen in the medium.[43] It is reasonable to consider that if the concentration of N_2 in the medium at the vicinity of the catalyst surface is not sufficient, then the yield of NH_3 cannot be high, however efficient the catalyst be. Of course, the N_2 adsorption efficiency of the catalyst will play a role besides N_2 solubility in the medium.

Ionic liquids are the most efficient in this respect to solvate N_2 gases in the medium. Gomes and co-workers worked with room temperature ionic liquid 1-butyl-3-methylimidazolium tetrafluoroborate, [bmim][BF_4],[44] and calculated the solubility of N_2 in terms of mole fractions of solute and Henry's law

constant given by eqn (7) and (8).

$$x_2 = n_2^{liq}/(n_1^{liq} + n_2^{liq}) \qquad (7)$$

where n_2^{liq} is the amount of solute dissolved in the ionic liquid and n_1^{liq} is the total amount of ionic liquid.

$$K_H = \lim_{x_2 \to 0} \frac{f_2(p, T, x_2)}{x_2} \cong \phi_2(p_{eq}, T_{eq})p_{eq}/x_2 \qquad (8)$$

where K_H is Henry's law constant, f_2 is the fugacity of the solute and ϕ_2 is the fugacity coefficient of the solute calculated in the usual way, p and T are the pressure and temperature of gaseous solute present in the gas bulb and p_{eq} and T_{eq} are the equilibrium pressure and temperature respectively.

This study showed that this ionic liquid electrolyte was able to solvate N_2 with $x_2 = 6.076$ and $K_H = 1646$ at room temperature. [bmim][BF$_4$] and 1-butyl-3-methylimidazolium hexafluorophosphate [bmim][PF$_6$][45] are widely used for this solubility study. The same group further worked on 1-alkyl-3-methylimidazolium ($C_n$mim, n = 2, 4, 6) tris(pentafluoroethyl)-trifluorophosphate ionic liquids (eFAP) and confirmed that the improved solubility of gases is due to the interaction of the solute (N_2) with the polar part of the ionic liquids as proved by the enthalpies of solvation and the site–site solute–solvent radial distribution functions using molecular simulation.[46] They further extended their finding to arrive at a point that ionic liquids with partial fluorination on the cation were found to increase CO_2 and nitrogen mole fraction solubility up to 50% compared to their hydrogenated counterparts.[47] Basically, perfluorinated organic liquids have a backbone of strong C–F bonds that cause a loss in molecular flexibility and a decrease in polarity, which in turn help to solvate the gas molecules facilely.[48] While Gomes et al. explored the anionic effect and showed a 30% increase in N_2 solubility from [C$_8$mim][NTf$_2$] ([NTf$_2$] is the bis(trifluoromethanesulfonyl)imide ion) to [C$_8$mim][BETI] ([BETI] is the bis(pentafluoroethanesulfonyl)imide), Noble et al. examined the influence of the imidazolium cation and found that the N_2 solubility decreased by approximately 36% due to the polar nature of the nitrile group.[49] To implement this strategy into the field of NRR, MacFarlane and group worked on [C$_4$mpyr][eFAP] and [P$_{6,6,6,14}$][eFAP] ionic liquids for NRR,[50] having a N_2 solubility of 0.20 mg g^{-1} and 0.28 mg g^{-1} respectively. The current density and yield were found to be more with the [C$_4$mpyr][eFAP] IL due to its lower viscosity, which supports higher mass transport while the F.E. was better for [P$_{6,6,6,14}$][eFAP] (60%). From theoretical calculations it was derived that N_2 was likely to interact with the F-atoms and greater the charge delocalization over the anionic and cationic part of the ionic liquids, better will be the interaction of the F-ends with N_2 and higher will be the N_2 solubility. Keeping this issue in mind, they further synthesized a series of phosphonium-based ILs with highly fluorinated anions, which displayed high N_2 solubility and all were found to be promising towards NRR.[51] This is a wide research field on its own and there is much scope to implement these ionic liquids in NRR in a better optimized way so that along with high F.E., the yield and production rate of NH_3 could be simultaneously improved.

3.2 Restriction of HER toward improved F.E. for NRR

Most of the times, the performance of the catalysts towards NRR is receded by an alarming issue which is the competitive hydrogen evolution process (HER).[52] The multiphase proton-coupled-electron process (NRR) not only involves a number of intermediates that are difficult to trace but also requires six electrons and six protons to completely get reduced to ammonia. This is unlike the case of HER, which involves a much faster kinetics with only two electrons and two protons.[53] Again, from thermodynamics point of view, the dissociation of the $N \equiv N$ bond is an energy intensive process. Therefore, although NRR and HER have the same working window, NRR suffers from a huge overpotential while HER becomes predominant. It is noteworthy that, at a low negative potential window, NRR becomes operative but with a lower current density. With the increase in the negative applied potential, the current density increases significantly, but the faradaic efficiency for NRR is drastically hampered by the rapid H_2 evolution.[1,54–56] Thus, with respect to the medium, accessible electrons and protons and material choice, it is crucial to maintain a proper balance so that either the working potential window for NRR could be increased or the achievable current could be more at a low negative potential. A detailed discussion regarding the above-mentioned points is provided below.

3.2.1 Influence of pH of electrolyte. For NRR, the pH of the electrolyte has an important role to play as it is directly linked to the concentration of the proton donor participating in the reduction process which consequently is related to the selectivity of NRR (Fig. 3a).[55] Usually, aqueous electrolytes include acidic electrolytes such as 0.1 M HCl and 0.05 M H_2SO_4, neutral electrolytes such as 0.1 M phosphate buffer solution (PBS), 0.5 M LiClO$_4$ and 0.1 M Na$_2$SO$_4$, and alkaline electrolytes such as 0.1 M NaOH and 0.1 M KOH.[6,57–59]

Centi et al. studied the effect of pH of electrolytes on ammonia selectivity using Fe$_2$O$_3$-CNTs under different pH of 0.6 (0.25 M KHSO$_4$), 7 (0.25 M K$_2$SO$_4$), 9.4 (0.5 M KHCO$_3$), and 13.7 (0.5 M KOH).[60] It was found that with the rise in the pH value the NRR FE increased and the maximum FE was obtained in the case of 0.5 M KOH (0.164%) which was almost two times more than that for 0.25 M KHSO$_4$ (0.075%). Likewise, for Mo$_2$C nanodots anchored on carbon cloth in a proton rich electrolyte (pH = 2), a low FE of 1.6% was obtained as compared to that in a proton suppressed electrolyte with FE = 7.8% (pH = 3).[61] In addition to this, Wu et al. revealed in their study that the nanoporous N-doped carbon catalyst showed better selectivity for NRR in the case of 0.1 M KOH than in 0.1 M HCl.[62] These studies conclude that high pH electrolytes with less proton availability lead to superior NRR selectivity due to the sluggish HER process.

The neutral PBS electrolyte with limited proton availability may be favourable in hindering the H_2 generation. Recently, Feng et al. demonstrated that the Pd/C catalyst in the neutral PBS electrolyte was more selective towards NRR than in acidic or basic media due to restricted HER.[63] Also in the case of the Fe/Fe$_3$O$_4$ catalyst the same trend is followed.[64] Additionally, the pH of the medium determines whether H_2O (basic medium) or
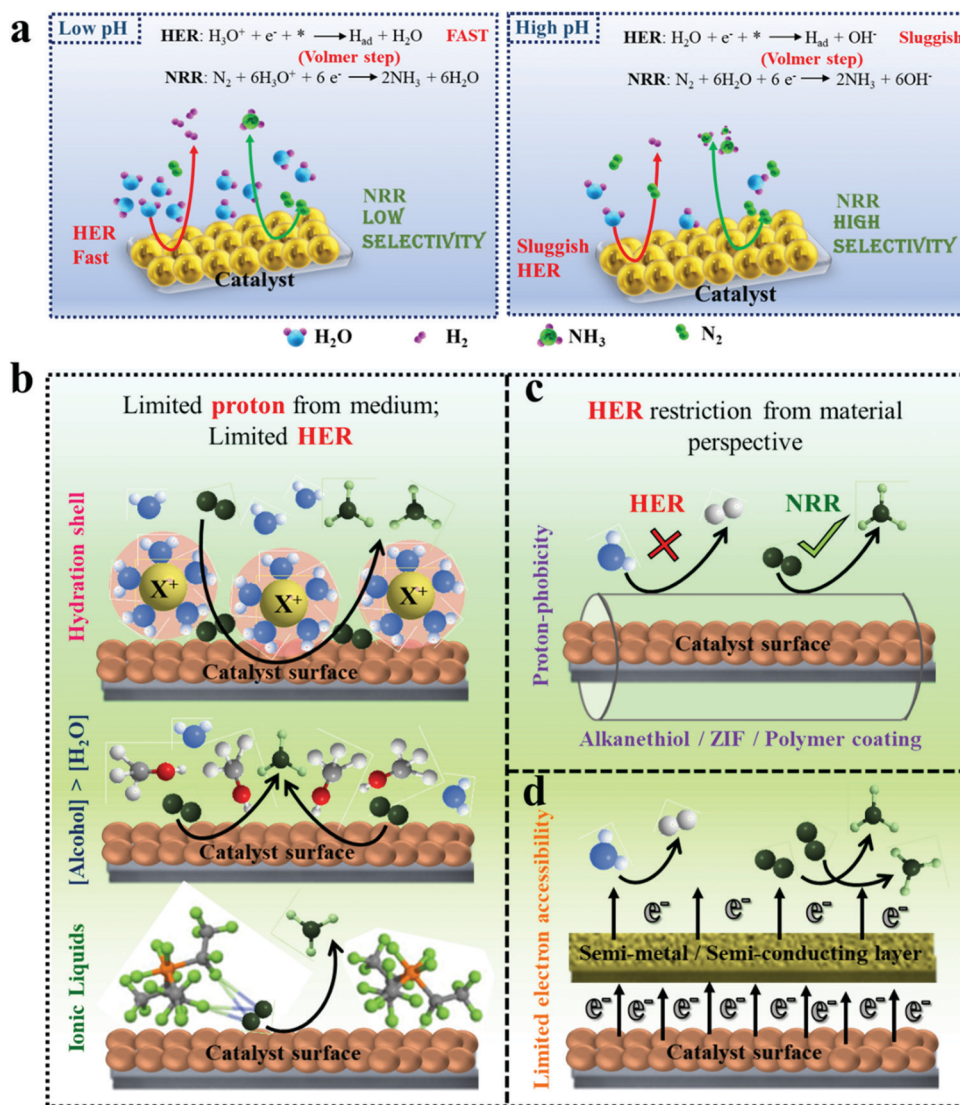
Fig. 3 Schematic representation of HER suppression. (a) Effect of pH on dominant NRR over HER. (b) Limiting proton source in the medium, restricting HER. The image of the ionic liquid has been reproduced with permission from Zhou *et al.*,[50] Copyright 2017, Royal Society of Chemistry. (c) Hydrophobic coating over the material to prevent HER. (d) Surface/semi-metal or surface/semi-conductor heterostructure inhibiting HER kinetics.

H_3O^+ (acidic medium) would act as proton donor during NRR (Fig. 3a). The Volmer step in the HER mechanism involves a high energy barrier for water dissociation in neutral and basic pH which is not the case in acidic medium.[65] Therefore, the HER process in alkaline and neutral electrolytes is more sluggish than in acidic electrolytes because of the restricted Volmer step. It is also to be noted that the pH of the electrolyte and selectivity towards NRR may be limited due to the cell configuration and catalyst.[66] Still there is a need to explore the effect of pH of the electrolyte and the local pH gradient around the catalyst for deep understanding of NRR selectivity.

3.2.2 Control over electron and proton accessibility. As already mentioned above, the kinetics of NRR is limited due to the faster HER kinetics. Nørskov and co-workers have confirmed that while HER is dependent on the proton and electron concentration by first-order, NRR is independent of the same as shown in eqn (1) and (2).[67] Naturally, if the electron and proton

accessibility could be limited either from the medium or from the material respectively, NRR could be facilitated over HER.

$$HER \propto [H^+]^1[e^-]^1 \qquad (9)$$

$$NRR \propto [H^+]^0[e^-]^0 \qquad (10)$$

3.2.2.1 Control over proton accessibility from medium. One of the vital components of any electrocatalytic process is the working electrolyte, which provides the platform for the reactions to occur. Generally, aqueous electrolytes are used for an ambient NRR process. However, in the case of acids like HCl, H_2SO_4, $HClO_4$ and H_3PO_4, the proton sufficiency cannot be controlled in the medium and that is why it is more favourable to use the corresponding salts. The presence of alkali metal cations like Li^+, Na^+ and K^+ favours the NRR process owing to their tendency to form solvation shells, and hence steric effects.

Review

Materials Advances

Several groups have investigated the role of cations in reinforcing the NRR kinetics[68].[42] It has been found both theoretically and experimentally that, the smaller is the size of the cations, such as in the case of Li^+, the affinity to form a hydration shell is maximum, which thereby increases the transfer barrier for the H_2O molecules close to the catalyst surface restricting the water splitting process. After a systematic investigation, Rondinone and co-workers confirmed that Li^+ in the medium outperformed Na^+ and K^+ with respect to NRR F.E. at different applied potentials like −0.8 V, −1.0 V and −1.2 V (vs. RHE) over an N-doped carbon nanospike (CNS) catalyst.[69] They also showed that the F.E. dropped remarkably as the size of the alkali metal ion increased from Li^+ to Na^+ to K^+. Not only the size of the cation, the concentration of the cation was also found to play a role in NRR F.E. – Yan et al. found that with the increase in the cation (K^+) concentration in the electrolyte from 0.2 to 1.0 mol L^{-1}, higher degree of the solvation layer over the surface of a bismuth nanocrystal (BiNC) catalyst could be achieved, which significantly retarded the migration of the protons in the electrical double layer (EDL). This led to an increase in the current density and thus F.E. for the NRR from 9.8 to 67%.[42] This trend and activity of alkali metal cations were irrespective of the catalysts and besides suppressing HER, K^+ was also able to promote N_2 adsorption on the catalyst surface.[70]

Besides this, another approach to limit the proton access in aqueous electrolytes is by using an optimum concentration of methanol/2-propanol in water.[71,72] While Kim et al. showed that 2-propanol/water (9:1 v/v) brought about effective NRR than the all-aqueous electrolyte, Ren et al. showed that, at 0.16% water volumetric content in the water–methanol medium, the availability and dissociation process of water got substantially restricted, accompanied by an expanded electrochemical window and inhibited HER. In this work by Ren et al., at −1.2 V vs. Ag/AgCl, the methanol-enabled electrolyte recorded a high NRR F.E. of 75.9 ± 4.1% and an ammonia yield rate of 262.5 ± 7.3 μg h^{-1} mg_{cat}^{-1} (FeOOH/CNTs), ~8-fold enhancement than that obtained in a 0.1 M KOH aqueous electrolyte. The reason is that, at an optimum methanol content, methanol is able to initiate intermolecular H-bonding with the water molecules, which in turn makes it difficult to dissociate the O–H bond of water molecules (suppressed Volmer step of HER). They also showed that, methanol could surpass other organic electrolytes like ethanol, propanol, butanol and dimethyl sulfoxide with water. Tsuneto et al. tried to completely ignore water molecules yet achieve remarkable NH_3 formation efficiency by incorporating Li^+ (0.2 M $LiClO_4$) into the organic electrolyte (tetrahydrofuran/ethanol (99:1 v/v)) on some metal electrodes. Lithium was found to act as a mediator to produce ammonia with a higher current efficiency (48.7%) when the electrolysis was conducted under a high pressure of N_2 (50 atm).[73] Contrary to this, ionic liquid (IL) electrolytes serve as a special candidate in solvating N_2 and achieving high F.E. for NRR up to 60%.[50,74,75] The control one could have in terms of electrolyte medium to limit the proton accessibility is schematically shown in Fig. 3b.

3.2.2.2 *Control over proton migration at the material–medium interface.* From a material perspective, in order to prevent the H_2O migration on the material surface, several researchers have sought the help of hydrophobic coatings over the active sites.[58] The use of alkanethiols over the catalysts like MoS_2 or Cu served as a hydrophobic layer inhibiting HER and promoting different electrolytic processes like NRR and CO_2 reduction.[76] Besides this, hydrophobic coatings around Au surfaces were also proved to have a benign effect on the energy efficiency of NRR.[77] Similarly, Ling et al. used a zeolitic imidazolate framework (ZIF) coating on the surface of a Ag–Au catalyst to suppress the HER activity of the catalyst with a 4-fold improvement for the NRR F.E.[78] As the ZIF layer is porous, to further prevent H_2O diffusion through the pores, they coated the ZIF with an oleylamine layer, which further inhibited the HER process.[79] Likewise, Wang and co-workers designed highly dispersed Au nanoparticles (active species) coated with a porous poly(tetrafluoroethylene) (PTFE) framework (hydrophobic layer).[80] The PTFE modified surface of the Au catalyst enabled N_2 diffusion to have sufficient N_2 molecules at the surface of Au nanoparticles for their subsequent reduction. Owing to the hindered H_2 evolution, the catalyst presented a considerably increased NRR F.E. in contrast to the original Au nanoparticles. More recently, Liu et al. reported a three-layered unique catalyst where the active interlayer of vacancy-rich $ReSe_2$ was sandwiched between two layers of hydrophobic carbon fibres.[81] In all these cases, the hydrophobic coating efficiently lowered the coverage of H_2O molecules on the surface of the active site to impede the HER kinetics, rendering superior NRR selectivity (Fig. 3c).

3.2.2.3 *Control over electron accessibility by catalyst engineering.* As already mentioned above, HER is dependent on the available electrons, while NRR and its corresponding NH_3 production efficiency are not affected by this. Keeping this issue in mind, upon limiting the electron sufficiency from the material surface, HER could be sufficiently suppressed (Fig. 3d) as shown by Qiao et al. They adopted an interface engineering strategy on 2D mosaic Bi nanosheets that featured a relatively large charge-transfer resistance of ~300 Ω, indicating a restricted electron transfer rate. As a result, HER was retarded delivering a high NRR F.E. of 10.46% at −0.8 V (vs. RHE).[82] Similarly, Sn-based catalysts were explored by Biswas et al. where they experimentally as well as theoretically demonstrated a suppressed HER on the Sn site of SnS_2 at the NPG@SnS_2 interface, promoting selective NRR with 49.3% F.E.[83,84] Röpke et al. fabricated their catalyst surface with conductive polyaniline (PAN) where they tuned the thickness of the PAN coating and thus controlled the electron accessibility and hence the kinetics of the NRR process.[85] Additionally, PAN could also accelerate the adsorption of N_2 molecules and their intermediates.[86] Similarly, other conductive polymers like polyimide and polypyrrole could also be used to drive forward NRR by slowing down the transfer rate of the electron flux from the catalyst surface to the adsorbed reactants.[4]

3.2.3 Material specificity. During NRR in aqueous medium, a parasitic reaction HER can go sideways. This is because H atoms get easily adsorbed on the catalyst surfaces in contrast
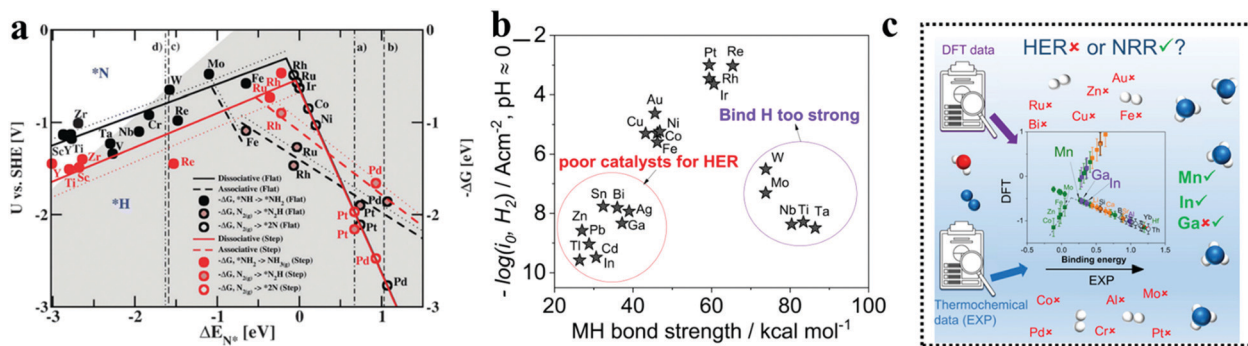
Fig. 4 (a) Volcano plot for the NRR on metal surfaces with specific mechanistic assumptions. A shaded area in the plot represents the overlaid volcano diagram for the HER counterpart. Reproduced with permission from ref. 189, Copyright 2012, Royal Society of Chemistry. (b) NRR over HER selectivity plot at pH 0, 4, and 14; volcano plot of HER. Experimental exchange currents of HER *versus* MH bond strengths (heat of adsorption of H_2 gas) for different metals (M), where the data are taken from Trasatti (1972). (c) Overview of selectivity of metals for NRR over HER from DFT as well as experimental point of view. Reproduced with permission from ref. 190, Copyright 2020, Elsevier B. V.

to N_2 molecules leading to evolution of H_2 eventually, lowering the selectivity of NRR.[87,88] So, the catalysts must be designed with the strategy of suppressing HER by decreasing the probability of adsorption of H atoms. Norskov *et al.* did a theoretical study to calculate the free energy of adsorption and reduction of N and H atoms on the surfaces of extensive metals in acidic medium.[89] It was observed that transition metals (Fe, Mo, W, Rh) showed high activity for NRR but they also had a tendency to adsorb H atoms (Fig. 4a). There are a few early transition metals (Sc, Ti, Zr, Y) that exhibited stronger binding of N atoms than H atoms. Following this, these metals and their corresponding complexes like TiO_2 nanosheets on Ti foil,[90] $Ti_3C_2T_x$ MXene nanosheets,[91] Y_2O_3 nanosheets, ZrO_2 nanoparticles,[92] *etc.* were obtained as they are electrochemically active for NRR. Although Sc-, Y-, Zr-, and Ti-based electrocatalysts have less binding ability for H atoms, their intrinsic NRR activity (FE ≤ 5%) is poor. Therefore, huge efforts are being made to improve their intrinsic NRR activity. Recent studies on single atom catalysts (SACs) are getting wide attention due to maximum atom-utilization and unsaturated coordination configuration in NRR due to suppression of HER (Fig. 4b and c).[93,94]

4. Transition metal borides (TMBs)

Transition metal borides or simply MBenes are an emerging class of catalysts, still in infancy in the field of NRR. Owing to the strong M–B and B–B covalent bonds, these catalysts offer high chemical and thermal durability and provide a high active surface area as compared to metal nitrides and carbides. As the composition of metal borides can vary over a wide range, they can act as metals/semiconductors/insulators in terms of electrical conductivity as per the requirement.[95–97] Several computational studies have been done for different groups of MBenes to shed light on the choice of T.M with best NRR performance and to deduce an estimation regarding the NRR mechanism being followed (Fig. 5a and b). The TMBs used for NRR have been summarized in Table 1. A study by Li *et al.* showed that among the T.M (Sc, Ti, V, Cr, Mo and W) boride monolayers, VB, CrB, and

MoB with the onset potentials of −0.396, −0.277, and −0.403 V, respectively, were screened out to be more effective for NRR (Fig. 5c). The VB monolayer was ascertained to follow the alternating pathway with the end-on configuration while CrB and MoB were more compatible to follow the mixed I pathway with the end-on and side-on configurations respectively (Fig. 5d and e).[98] However, there is no particularity in terms of mechanism for different MBenes as shown in Fig. 5f and g. In addition to CrB and MoB, Guo *et al.* also suggested that WB, Mo_2B, V_3B_4 and a few mixed metal borides like $CrMnB_2$ and $CrFeB_2$ act as a HER suppressant and have intrinsic basal plane activity for NRR with limiting potentials ranging from −0.22 to −0.82 V.[99] Zhao's group also included TiB in the preference list for NRR, which was later experimentally proved by Luo and co-authors using a sputtered TiB_2 film to enable superb electrochemical N_2 reduction.[100] It is noteworthy to mention that Ma and co-workers worked on ternary metal borides like molybdenum aluminum boride (MoAlB) single crystals experimentally, which afforded an NH_3 yield of 9.2 μg h^{-1} cm^{-2} mg^{-1}$_{cat.}$ and a faradaic efficiency of 30.1% at a low overpotential of −0.05 V *versus* RHE in alkaline solutions. The 3p/2p bands of Al/B were considered to interact with the N-orbitals and with the synergism of Mo, this catalyst successfully suppressed HER on its surface to give a reasonably fair faradaic efficiency for NRR.[101]

The beauty with this material is that one can have precise control over the choice of metal to involve the metal site as well as the boride counterpart in the activity during NRR. The interaction between boron and nitrogen is a well-known concept and has been illustrated in Fig. 1a. The strong coupling between the 2p orbitals of boron and nitrogen makes boron a favorable site for N_2 adsorption[17] (Fig. 6a–c). In the work by Cheng *et al.*,[102] they have theoretically computed that the boron site for TaB is the active center for NRR, while the Fe site for FeB is more likely to carry out N_2 reduction, but have a tendency to undergo H_2 poisoning, affecting NRR kinetics. It is however considered that the B site is more active towards NRR than the metal sites for most of the M-benes.[103] With respect to metal diborides, Yang *et al.* explored the electrocatalytic activity of FeB_2, RuB_2 and OsB_2 for the N_2 reduction reaction (NRR) by first principles
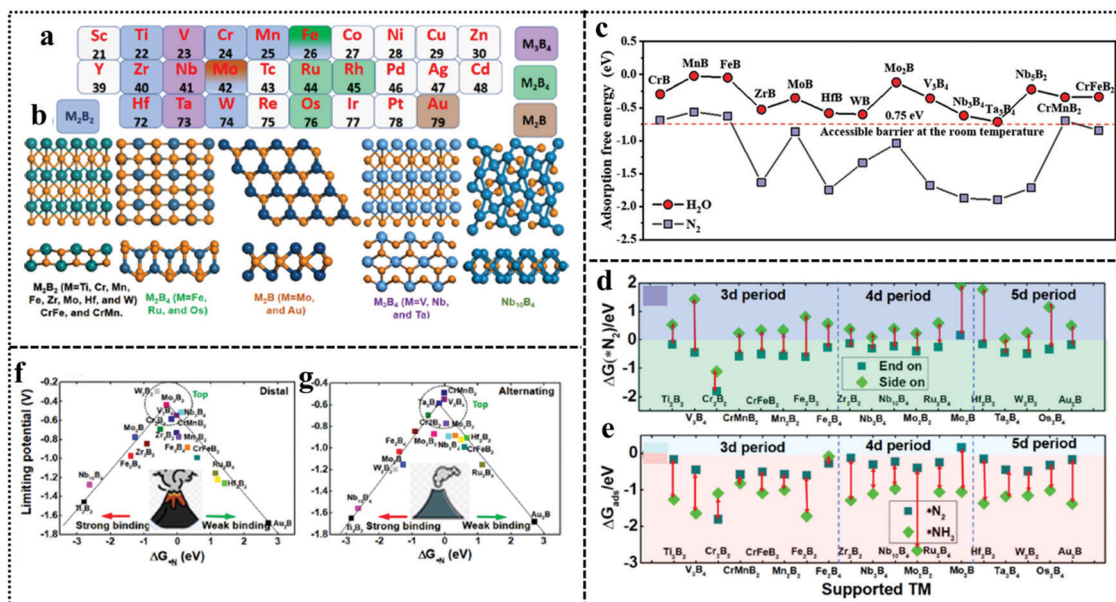
Fig. 5 (a) All MBenes for which both experimental and theoretical studies have been proposed are listed in the periodic table of elements. The stable structural prototypes of MBenes are indicated in different colors. (b) Top and side views of calculation models for different MBene structural prototypes that were built. Reproduced with permission from Long et al.,[191] Copyright 2021, American Chemical Society. (c) Computed free energy of adsorption of H_2O and N_2 on different Mbenes. Reproduced with permission from Guo et al.,[192] Copyright 2020, Wiley-VCH Verlag GmbH. (d) Adsorption energy of end-on and side-on binding configurations of N_2 on the Mbene surfaces. (e) Adsorption energies of N_2 and NH_3 on the surfaces of MBenes considered. (f) NRR volcano plot of MBenes with a descriptor of ΔG^*N via the distal path, (g) NRR volcano plot of MBenes with a descriptor of ΔG^*N via the alternating path; the data points that stand near the top of the volcano plot are highlighted. The arrows to the left represent strong adsorption of $*N$, and the arrows to the right mean weak adsorption of $*N$. Reproduced with permission from Long et al.,[191] Copyright 2021, American Chemical Society.

Table 1 A brief summary of transition metal borides used for NRR

Catalyst	Electrolyte	F.E. (%)	NH_3 yield rate	Potential (vs. RHE)	Ref.
MoAlB SCs	0.1 M KOH	30.1	9.2 µg h^{-1} cm^{-2} mg$_{cat}^{-1}$	−0.05 V	101
a-FeB$_2$ PNSs	0.5 M LiClO$_4$	16.7	39.8 µg h^{-1} mg$_{cat}^{-1}$	−0.2 V, −0.3 V	104
TiB$_2$	0.1 M HCl	11.37	1.75×10^{-10} mol s^{-1} cm^{-2}	−0.3 V	100

calculations and found that these M-benes with surface B atoms as the active sites exhibited superior activity (with low onset potentials in the range of −0.03 to −0.26 V) for the NRR than those with metal active sites. Being a newly emerging field, there is a lot of controversy concerning the active sites of this material. For example, in contrast to the work by Yang et al., Chu et al. for the first time experimentally demonstrated the synthesis and NRR with amorphous FeB$_2$ porous nanosheets and with the help of theoretical studies confirmed the active site to be Fe (Fig. 6d) and further revealed that amorphization lifted up the d-band center of the metal centre in FeB$_2$ to boost d-2π^* coupling between the active Fe site and the $*N_2H$ intermediate, resulting in enhanced $*N_2H$ stabilization and reduced reaction barrier. This resulted in an NH$_3$ yield of 39.8 µg h^{-1} mg^{-1} (−0.3 V) and a faradaic efficiency of 16.7% (−0.2 V), significantly outperforming their crystalline counterpart, as can be seen from their NRR performance (Fig. 6e and f) and the full free energy reaction pathway (distal pathway in Fig. 6g). They also showed that, for the amorphous FeB$_2$, the desorption of the first NH$_3$ is the rate determining step.[104] Another theoretical report by Wang et al.

followed this trend for Mo$_2$B$_2$, where Mo was identified as the active site and its 4d-orbital electrons were particularly held responsible for the NRR process on the material surface. The good electrical conductivity of the material initiated faster NRR charge-transfer kinetics.[105] The potential determining step being $*NH^2 + H^+ + e^- \rightarrow *NH_3$, this catalyst followed the alternating pathway for NRR at the cost of a low energy barrier. However, an elaborate study by Li et al. on Fe-based borides suggested that, Fe and B can synergistically act as active sites for NRR. Not only that, M–M and B–B interactions can optimize the catalyst performance towards NRR mostly from the bulk than single atom sites. Thus, mass loading plays a very important role in tuning the activity of M-benes, with higher mass loading resulting in more improved performance. They also demonstrated that different phases of the catalysts exhibit different NRR mechanism pathways like the most favorable NRR paths for FeB and FeB$_2$ are the alternating and dissociative paths, respectively.[106] Mostly, for the M-benes where B serves as the active site, over a series of transition metals, mostly the enzymatic and consecutive reaction mechanisms are followed, while with the metal active
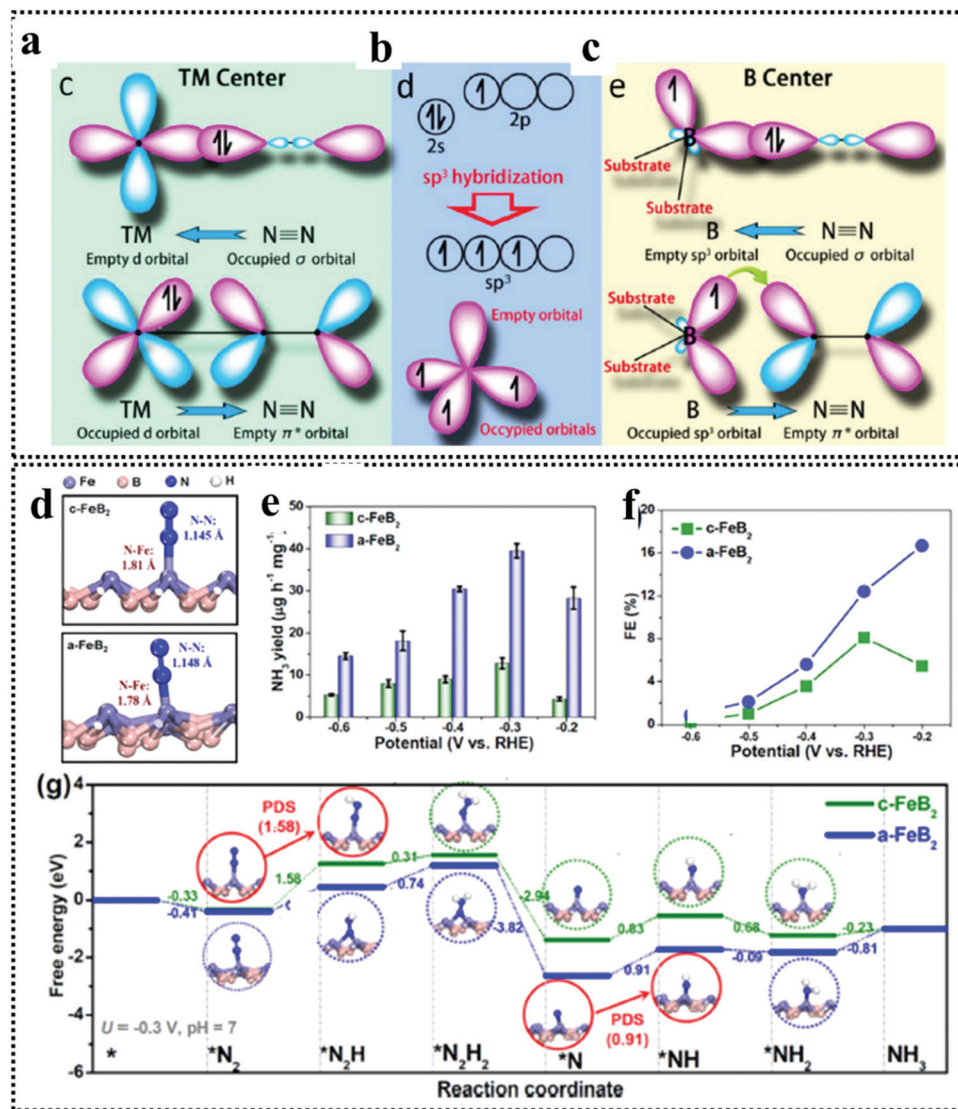
Fig. 6 (a) Simplified schematic of N₂ bonding to TMs. (b) Electronic configuration of the pure B atom and B atom with sp^3 hybridization. (c) N₂ binding motifs to the B atom on the substrate. Reproduced with permission from ref. 193, Copyright 2018, American Chemical Society. (d) Optimized structures of c-FeB₂ and a-FeB₂ after N₂ adsorption. Comparison of (e) NH₃ yields and (f) FEs of c-FeB₂ and a-FeB₂ PNSs at various potentials. (g) Free energy diagrams of NRR reaction pathways on c-FeB₂ and a-FeB₂ at $U = 0.3$ V and pH = 7. Reproduced with permission from ref. 104, Copyright 2021, Elsevier B. V.

sites, alternating, distal and enzymatic pathways are more preferred to achieve NRR overpotential (η_{NRR}) < 1 as shown in Fig. 1b.

Unlike the MXenes where surface oxidation is a major concern to block the active sites, once oxidized, these MBenes can catalyze NRR *via* the self-activating process, reducing O*/OH* into H₂O* under reaction conditions, and favoring the N₂ electroreduction. As a result, the exceptional activity and selectivity, high active area ($\approx 10^{19}$ m^{-2}) and antioxidation nature render these MBenes pH-universal catalysts for NH₃ production without introducing any dopants and defects. However, vacancy engineering is also explored in the M-bene materials. Both cationic and anionic vacancies are rendered by Li's group and Chen's group respectively and assembled with single atom crystals to bring about more efficiency in the NRR performance by the combined advantages of SACs and M-benes

with defects. Re and Os implanted into Mo vacancies of Mo₂B₂O₂ nanosheets (Fig. 7a–c) were found to possess remarkable catalytic activity with relatively low barrier values of the potential-determining step (PDS) of 0.29 and 0.32 eV, which are lower than that of the single Ru atom decorated on Mo₂CO₂ (0.46 eV).[107] Chen's group predicted that Ti single atom doped B-vacant VB₂ (Ti@VB₂) having a limiting potential of −0.61 V for NRR is the most effective among all the other single atom doped 2D-TMBs with a B vacancy.[108]

However, there is no parity in the mechanistic performance of the different M-benes. It is absolutely dependent on the metal being used and the phase of the boride being formed. It is however easy to simulate metal as well as mixed-metal borides but for practical experimentation, it is very crucial to maintain appropriate conditions in order to obtain the phase-specific M-benes. Like for example, CoB and Co₂B are the most
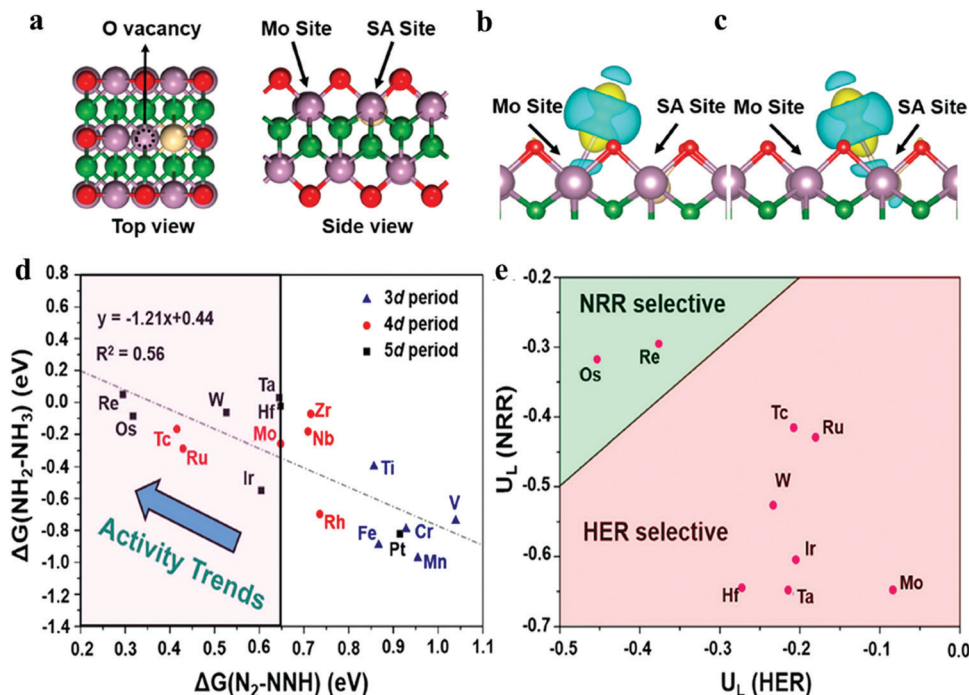
Fig. 7 (a) Top and side views of the structure of SA-doped $Mo_2B_2O_2$, where red, purple, green, and white balls represent O, Mo, B, and doped SA, respectively. The charge density difference of N_2 adsorption geometries in the O vacancy of SA-doped $Mo_2B_2O_2$: (b) Mo site and (c) SA site. (b) Reactivity screening of $Mo_2B_2O_2$–SA systems for NRR, according to the linear distribution with regard to the free energy changes of the first and the last hydrogenation steps ($\Delta G(N_2$–NNH) and $\Delta G(NH_2$–$NH_3)$), with $Mo_2B_2O_2$–Mo (the pure $Mo_2B_2O_2$ with O vacancy) as the boundary line. (c) Calculated potential *vs.* SHE for HER (U_{*H}) and NRR (U_{*NNH}) for selectivity screening. The dashed line represents $U_{*H} = U_{*NNH}$. Reproduced with permission from ref. 107, Copyright 2020, American Chemical Society.

widely synthesized M-benes, applied for different energy applications other than NRR.[109] But the synthesis strategy used there may not work accurately for other metal borides, requiring different experimental conditions. Thus, it is indeed important to optimize the conditions and properly characterize the material before going deep into the electrochemical performance for NRR. However, there is enough room for exploration of this category of catalysts as only three to four experimental reports are available on NRR with FeB_2, MoAlB, TiB_2 and Ti@VB_2.

5. Transition metal carbides (TMCs)

Transition metal carbides (TMCs) have been shown to be effective catalysts for the NRR, in addition to transition metal oxides (TMOs) and transition metal nitrides (TMNs).[110–115] According to recent studies,[116] adsorption capacity for N_2 is greatly influenced by elemental electronic properties, since only atoms that have partially filled d-orbitals with correct symmetry can synergistically acquire electrons from N_2 and donate back to N_2. Notably, the p-back-donation method has the capability of effectively weakening N–N bonds while concurrently strengthening metal–N bonds.[117] To activate the N–N bond, it is necessary to fabricate electron-donating electrocatalysts that include an abundance of catalytic activation sites. In accordance with the well-known d-orbital hypothesis,[118] transition metal carbides (TMCs) display an electronically favorable architecture

and adsorption[119] exhibiting intrinsic noble-metal-like behavior because of the dense d-orbitals of the transition metal, which allows for much more p-back donation possibilities for the adsorbates.[120] The capacity to donate electrons to the N_2 p* antibonding orbitals and cleave the N–N bonds is further enhanced by creating anion vacancies with localized electrons. Moreover, vacant d-orbitals of transition metal carbides have excellent adsorption capacity.[121] The sp-hybridized state of the transition metal, which exists in the carbides, is delocalized on the surface, where it will interact with the d-state of the transition metal as well as the s-state of carbon. To effectively activate the N–N triple bond with NRR catalytic activity, a highly occupied orbital affords more possibilities for reverse donation to the p orbital of N_2.

Moreover, the two-dimensional transition metal carbides are a novel class of 2D materials that have sparked current interest.[122] Metal carbide research began in 2011 with the discovery of the first Ti_3C_2 compound, which has grown to a family of over 30 members.[123] In the report by Sang *et al.*,[124] the authors have grown a TiC single layer on a Ti_3C_2 substrate to introduce a 2D Ti_5C_4 material in the field of electrocatalysis. But the prospect of 2D transition metal oxides/nitrides/carbides as possible electrocatalysts toward NRR has only been briefly considered from a theoretical standpoint.

It is believed that Mo carbides (MoC) would be useful for a wide range of electrochemical energy conversion applications, including NRR, because of their comparable d-band electrical

density to that of metal Pt.[125,126] The transition metal molybdenum (Mo) has been explored for converting N_2 gas to NH_3. In accordance with DFT calculations, the bond strength of nitrogen (N_2) trapped on the Mo domains is too strong to allow the formation of ammonia (NH_3) upon the Mo active sites.[127] Bonding with non-metals including carbon atoms with high electronegativity might reduce the Mo and N_2 interaction, improving N_2 fixing efficiency. Consequently, molybdenum carbides were studied as photocatalytic materials for N_2 fixation. Furthermore, the MoC architecture has been utilized as an electrocatalyst for N_2 reduction with a lower NRR (0.54 V),[128] while, with a 0.3 V potential at its (1 1 1) plane, cubic MoC has been reported as a noble NRR electrocatalyst, proving the MoC material's utility for NRR.[128] Additionally, a composite made of oxygen-containing molybdenum carbides embedded in nitrogen-doped carbon layers was created by Qu et al. using dopamine and molybdate as precursors.[129] A synergistic combination among O–MoC and N-doped carbon shells resulted in high catalytic activity (NH_3 production rate: 22.5 g mg h_{cat}^{-1}), selectivity (95%) (HCl solution: 0.5 m Li_2SO_4), and stability (95%) (HCl solution: 0.1 m Li_2SO_4). Interestingly, DFT simulations by Matanovic et al.[128] investigated cubic MoC as an electrode material for NH_3 production. However, on all MoC surfaces except MoC(111), H-atoms competed with N-atoms. It is possible that HER will be inhibited at low potentials on MoC(111), but this is not the case on any other surfaces. This is owing to the wider stability area of N ad-atoms relative to that of H ad-atoms. As a result of the presence of carbon vacancies, the hydrogen development and build-up of H ad-atoms can be reduced, indicating that the metal-to-carbon ratio can be increased while maintaining the same attraction for N ad-atoms as in MoC. By exposing to high hydrogen evolution conditions, Wang et al.[130] developed Mo_4C nanodots embedded in carbon nanosheets (Mo_2C/C) that served as a better NRR catalyst. Considering ambient circumstances, the as-prepared Mo_2C/C demonstrated outstanding catalytic activity with high NH_3 production (11.3 mg h^{-1} Mo_2C) and FE (7.8%). Further, their comparative test reduced the influence of hydrogen evolution to get the precise NRR activity of Mo_2C/C. The FE increased about 5-fold in the proton-suppressed condition compared to the NRR findings in the proton-enriched condition. Nevertheless, under a proton-suppressed state, the NH_3 production rate of Mo_2C/C was reduced significantly. Excessive HER suppression may increase NRR selectivity but reduce NRR activity. Thus a suitable proton donor is required. Mo_2C also exhibits more activity in HER than in NRR due to the presence of uncontrolled and diverse flaws, edges, and a mixture of distinct crystal facets that are present. A new 2D a-Mo_2C material with a strongly oriented (200) facet of the a-Mo_2C phase was proven by Sun and Li[131] as an NRR catalyst. Due to the Mo_2C's single crystal facet, this catalyst attained a phenomenal FE of 40.2%.

The electrocatalytic performance of Mo_2C nanodots embedded in ultra-thin carbon nanosheets (Mo_2C/C) was reported by Wang et al. to be remarkable for NRR.[130] Inside a 0.5 M Li_2SO_4 solution, NH_3 yield was 11.3 mg h^{-1} (pH = 2). The NRR technique utilizes Mo_2C nanodots as active center sites, as indicated by DFT and electronic state density calculations. The results showed that severe HER inhibition did not promote

NRR activity, showing that Mo_2C/C may execute NRR under HER circumstances. Mo_2C nanorods were produced and deposited on glassy carbon electrodes for electrochemical NRR. Mo_2C/GCE had good catalytic activity, yielding 95.1 mg NH_3 per mg_{cat} and 8.13% faradaic efficiency (0.1 M HCl at 0.3 V (vs. RHE)). A highly active surface, the (121) facet, of the Mo_2C nanorods successfully absorbed and activated N_2 as a result of its high surface activity. Besides Mo_2C, the researchers discovered cobweb-like MoC_6,[132] Cr_3C_2 nanoparticles,[133] and additional N_2 fixation catalysts.

However, TMC-based catalysts have limited NRR activity because their HER-active edges favor H-ad atoms over N-ad atoms. To address this issue, structural or component adjustments are required to improve NRR. To achieve effective NRR catalysis under high hydrogen evolution conditions, researchers synthesized molybdenum carbide nanodots embedded in ultrathin carbon nanosheets (Mo_2C/C). This unique inlaid arrangement reduces hydrogen overflow on the catalyst surface, allowing for increased N_2 diffusion. Using density functional theory, Li et al. discovered that the surface of molybdenum carbide may be terminated by hydrogen through the Volmer process.[127] Due to its moderate HER overpotential, huge DG_{max} (1.4 eV), and kinetic barrier (20.0 eV), H-covered Mo_2C was not an effective NRR catalyst. Consequently, molybdenum carbide has been reported hardly for NRR. In 2018, Cheng et al. examined the electrocatalytic activity of Mo_2C nanodots incorporated in carbon nanosheets (Fig. 8a).[130] They had a high NH_3 yield (11.3 mg h^{-1} mg_{cat}^{-1}) and faradaic efficiency (7.8%). To achieve actual NRR activity, the authors applied a hydrophobic carbon cloth instead of a hydrophilic one, and increased the pH from 2 to 3. When compared to the findings obtained under proton-rich circumstances, the faradaic efficiency obtained under proton-suppressed conditions was approximately five times higher (Fig. 8b), but the NH_3 yield was much lower (Fig. 8c), showing that an optimal proton donor is required for NRR to produce a large NH_3 yield. The extremely active surface of Mo_2C nanodots allows them to absorb and activate nitrogen (Fig. 8d). Also, the Mo_2C nanodots were equally enclosed in carbon nanosheets, reducing hydrogen coverage on the catalyst surface and increasing N_2 diffusion. On the other hand, Fang et al.[134] created Mo_2C nanodot coated 3D ultrathin macroporous carbon ($Mo_2C@3DUM-C$). $Mo_2C@3-DUM-C$ showed increased electron and mass transmission due to its three-dimensional ultra-thin macroporous carbon framework. At 0.20 V, $Mo_2C@3DUM-C$ demonstrated 9.5% NRR efficiency and 30.4 mg per h per mg_{cat} NH_3 yield. $Mo_2C@3-DUM-C$ also had high catalytic stability for NRR due to its geometrical and electrochemical stability. In another study, Qu et al. effectively synthesized oxygen-doped MoC nanoparticles encapsulated in N-doped carbon shells with adjustable core–shell nanomaterials (OeMoC@NC-T) for NRR[135] (Fig. 8e). OeMoC produced 22.5 mg per h per mg_{cat} NH_3 and had a faradaic efficiency of 25.1%. On the basis of reaction energies (vs. conventional hydrogen electrode), V_3C_2 and Nb_3C_2 were identified to be the most promising options. From a kinetic perspective, V_3C_2 had lower activation energy barriers (0.64 eV)
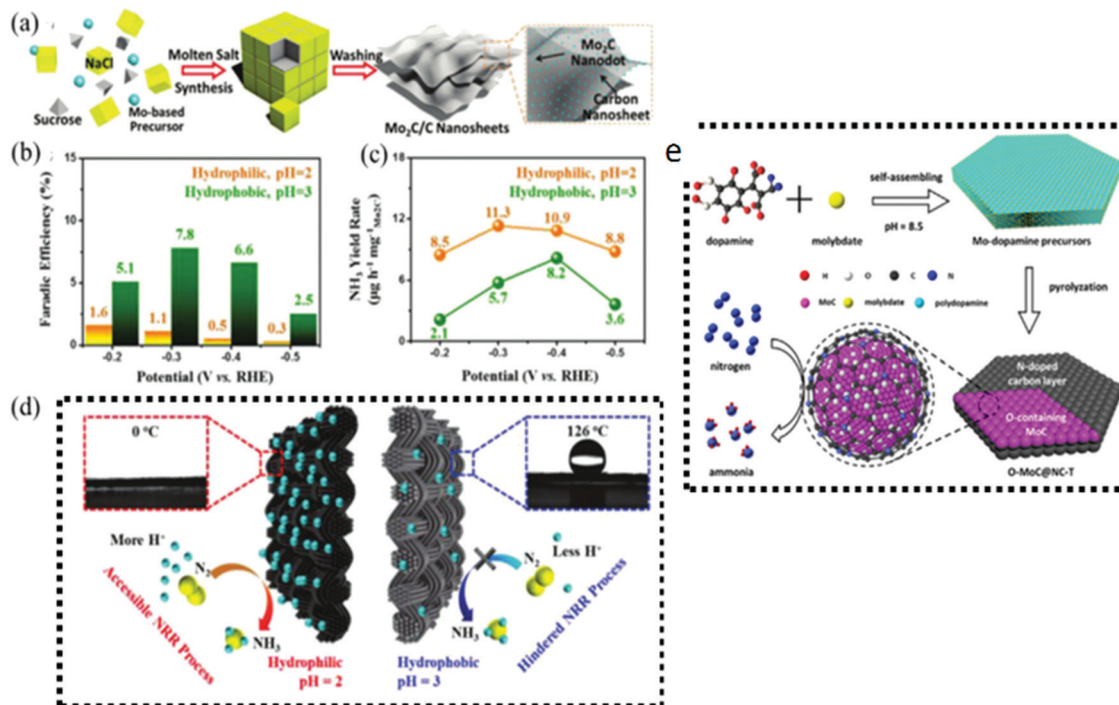
Fig. 8 (a) Schematic representation of the synthetic route for molten salt Mo_2C/C nanosheets. (b) Faradaic efficiency, (c) yield rate and (d) NRR mechanistic pathway of Mo_2C/C in proton-suppressed and enriched environments. Reproduced with permission,[130] Copyright 2018, Wiley-VCH Verlag GmbH. (e) Schematic illustration of the fabrication procedure of OeMoC@NC-T. Reproduced with permission,[135] Copyright 2019, American Chemical Society.

than Nb_3C_2, and its reaction profile was smoother with lower energy barriers for additional hydrogenation phases.[136] On the other hand, DFT calculations revealed that the central Ti atoms displayed the maximum adsorption of N_2 (1.344 eV) as compared to certain other sites such as O, C, and lateral Ti atoms. Thus, Ti_3C_2 supported by stainless steel mesh (SSM) obtained a maximum faradaic efficiency of 4.62% (0.1 V versus RHE) and an NH_3 yield rate of 4.72 µg h^{-1} cm^{-2}.[137]

Using an ultrasonic reduction method, Liu et al. created an accordion-like morphology of Au nanoparticle-anchored Ti_3C_2. At 0.2 V, Au/Ti_3C_2 produced 30.6 mg per (h mg) of NH_3 and had a Faraday efficiency of 18.34%.[138] The authors established that the high energy of N_2 adsorption on the interface among high-valence-state gold clusters and Ti_3C_2 represented the driving force for the breaking of triple N–N bonds, and that the overall activation energy threshold could be decreased by efficiently stabilizing N_2^* species while destabilizing $NH_2NH_2^*$ species via an alternate channel instead of the conventional one. As a consequence of the synergistic effect, $1T-MoS_2/Ti_3C_2$ composites demonstrated excellent stability, excellent durability, and remarkable NRR activity, with a faradaic efficiency of 5.26% and a nitrogen production rate of 36.28 mg h^{-1} mg_{cat}^{-1} at 0.35 V vs. RHE.[139]

5.1 MXenes and MXene derivative catalysts

MXenes have emerged as one of the foremost intensively explored novel materials. They possess excellent potential as active catalysts for catalytic conversion including environmental

remediation, due to their remarkable layered architecture, relatively high surface area, ample active sites, and superior chemical inertness. MXenes are intriguing catalysts for N_2 absorption as well as reduction, as their effectiveness has indeed been formerly forecast.[140,141] Recent developments illustrate MXenes or their derivatives in adsorbing, stimulating, and reducing nitrogen (N_2) to ammonia (NH_3) via electrocatalytic as well as photoelectrochemical nitrogen reduction reaction (NRR). Despite the conventional Haber–Bosch approach, which directly implements fossil fuels with highly energetic techniques, the electrochemical NRR is regarded as appropriate as well as environmentally acceptable for NH_3 production. Nevertheless, the NH_3 productivity and efficacy of NRR adopting MXene-based catalysts continue to be relatively insufficient to achieve real world applications. Consequently, a basic understanding of NRR pathways with their considerable limitations should be addressed for prospective advancements.

In this regard, several experimental investigations with comprehensive findings suggest that MXenes could function competitively with the reference Pt-, Co-, or Pd-based catalysts in converting N_2 to NH_3. Furthermore, one most significant benefit of MXenes as a catalyst is that certain chemicals included within seem to be earth-abundant. Owing to their affordability, the catalysis cost can indeed be severely decreased without affecting the effectiveness. Throughout NH_3 electrosynthesis, $Ti_3C_2/FeOOH$ displayed an excellent FE of approximately 5.78% at an exceptionally low potential, closer to that of Pt.[142] $Ti_3C_2T_x$ nanosheets besides binding with dimethyl sulfoxide (DMSO) as well acquired better electrochemical behavior

for nitrogen reduction, showing an NH_3 production of 20.4 mg h^{-1} mg$_{cat.}^{-1}$ with a FE of 9.3% in acid buffer.[143] Various forms of MXenes might be effectively utilized for the catalysts for the electrochemical NRR, e.g. V_3C_2 and Nb_3C_2, leading to maximal overpotentials of approximately 0.64 and 0.90 eV, respectively, and hence diverse MXene nanocomposites have also been published.[144] Significant modification techniques including improvement of MXenes via considerably improved synthesis with appropriate material compositions are being developed to enhance their applicability for N_2 catalyst purposes.

However, the NRR does have a slow kinetic response and therefore is inadequately generated. The emerging 2D MXene category is considered to be more competitive in aqueous medium, suppressing HER while promoting NRR. MXenes could be synthesized into much more efficient catalysts as well as coupled with other catalytic substances to produce hybrid materials. MXenes could be fabricated into thin films as 2D materials, strengthening their feasibility for implementation in devices. Conversely, the minimum quantity of material utilization and the minimal infrastructure are anticipated to be cost-effective in terms of hydrogen generation and its production rate. A similar approach can be adopted for NRR catalysts employing MXenes. Additionally, thin-film MXenes could be embedded into the reactors thereby potentially leading to low-cost NH_3 production. But it is still too early to draw such a definitive inference since in the attempt to reasonably develop the optimum MXene catalyst for NRR with practical implications, numerous tasks must be addressed. Table 2 summarizes the research paradigm carried out for N_2 reduction to NH_3 adopting various metal-carbides as well as MXene-based catalysts and its derivatives as an electrocatalyst.

6. Transition metal nitrides (TMNs)

For overall development of NRR, along with noble metals like Au, Pd, Rh, Ru, etc., various advanced transition metal electrocatalysts such as transition TMNs, TMCs,[130,145] TMOs[146,147] and TMBs[148,149] have attracted the attention in recent years. Among these, TMNs are of great importance due to their high conductivity, modulable electronic structures, good stability and cost efficiency. As explained above, for NRR, different types of mechanisms can be followed depending upon the system. TMNs follow the heterogeneous Mars-van Krevelen (MvK) mechanism, which makes these materials more promising as in this mechanism, the aforementioned two main challenges in NRR are overcome: (1) elimination of high energy required to break the triple bond of the N_2 molecule and (2) suppression of the parasitic HER.[150,151] Basically, in this mechanism, the N on the catalyst layer is electrochemically reduced to ammonia under ambient conditions and the so formed vacancies are replenished with gaseous nitrogen that regenerates the catalyst (Fig. 1e). Furthermore, the adsorption of gaseous N_2 onto the nitride catalyst is highly facilitated as the N-vacancy decorated on the nitride surface has high surface energy that solves the problem of low solubility of N_2 in water.[36,152,153]

Skulason et al. provided deep insights into catalysts especially into TMNs (FeN, CoN, NiN, RuN, RhN, PdN, OsN, IrN, CrN, VN, NbN, CrN) which are active and selective for NRR to ammonia following the MvK mechanism by theoretical investigations. The onset potential for NH_3 formation was calculated by DFT calculations via conventional AM, DM, and combination of these two mechanisms (AM-DM) and compared with the MvK mechanism to determine the lowest onset potential on the clean surface of TMNs.[154] Since adsorption of N_2 is an endothermic process, therefore, MvK is always favoured on TMNs. Out of the various TMNs, rocksalt VN and ZrN are found to be the most promising candidates due to the requirement of low bias for ammonia production and HER suppression. DFT presented that at the onset potential, the so formed N-vacancies get easily repaired with gaseous nitrogen

Table 2 Summary of metal carbides, MXenes and MXene derivatives for NRR

Catalyst	Electrolyte	FE (%)	NH_3 yield	Potential vs. RHE (V)	Ref.
α-Mo_2C	0.1 M Na_2SO_4	40.2	3.36 μg h^{-1} cm^{-2}	−0.55	174
Mo_2C@3DUM-C	0.1 M HCl	9.5	30.4 μg h^{-1} mg$_{cat}^{-1}$	−0.2	134
1T-MoS_2/Ti_3C_2	0.1 M HCl	5.26	36.28 μg h^{-1} mg$_{cat}^{-1}$	−0.35	139
Au/Ti_3C_2	0.1 M HCl	18.34	30.6 μg h^{-1} mg$_{cat}^{-1}$	−0.2	138
Mo_2C/C	0.5 M Li_2SO_4	7.8	11.3 μg h^{-1} mg$_{cat}^{-1}$	−0.3	130
Cr_3C_2@CNFs	0.1M HCl	8.6	23.9 μg h^{-1} mg$_{cat}^{-1}$	−0.3	133
Mo_3Fe_3C	0.1 M Li_2SO_4	27	72.5 mmol h^{-1} g$_{cat}^{-1}$	−0.05	101
Mo_2C/NC	0.1 M Na_2SO_4	12.3	70.6 μmol h^{-1} g$_{cat}^{-1}$	−0.2	175
1T-MoS_2@Ti_3C_2	0.1 M HCl	10.94	30.33 μg h^{-1} mg$_{cat}^{-1}$	−0.3	176
Surface-engineered Ti_3C_2	0.1 M KOH	7.01 (20 °C)	1.71 μg h^{-1} cm^{-2}	−0.2	177
		9.03 (60 °C)	12.46 μg h^{-1} cm^{-2}	−0.2	
$Ti_3C_2T_x$ (T $\frac{1}{4}$ F, OH) MXene nanosheets	0.1 M HCl	9.3	20.4 μg h^{-1} mg$_{cat}^{-1}$	−0.4	178
Fluorine-free $Ti_3C_2T_x$ (T $\frac{1}{4}$ O, OH)	0.1 M HCl	9.1	36.9 μg h^{-1} mg$_{cat}^{-1}$	−0.3	179
TiO_2/$Ti_3C_2T_x$	0.1 M HCl	8.42	26.32 μg h^{-1} mg$_{cat}^{-1}$	−0.6	180
Oxygen-vacancy-rich TiO_2/$Ti_3C_2T_x$	0.1 M HCl	16.07	32.17 μg h^{-1} mg$_{cat}^{-1}$	−0.45, −0.55	181
Ti_3C_2 MXene nanoribbons	0.5 M KOH	3.1	14.76 μg h^{-1} mg$_{cat}^{-1}$	−0.5	182
Hydroxyl-rich Ti_3C_2Tx QDs	0.1 M HCl	13.30	62.94 μg h^{-1} mg$_{cat}^{-1}$	−0.5	183
V_2CT_x MXene	0.1 M Na_2SO_4	4	12.6 μg h^{-1} mg$_{cat}^{-1}$	−0.7	184
Cu/$Ti_3C_2T_x$ MXene	0.1 M KOH	7.31	3.04 mmol h^{-1} cm^{-2}	−0.5	185
NeS-doped $Ti_3C_2T_x$	0.05 M H_2SO_4	6.6	34.23 μg h^{-1} mg$_{cat}^{-1}$	−0.55	186
Ni nanoparticles/$V_4C_3T_x$ MXene	0.1 M KOH	14.86	21.29 μg h^{-1} mg$_{cat}^{-1}$	−0.55	187

injected to the system and are not poisoned by oxygen or hydrogen from the aqueous electrolyte.[155,156]

Zhang et al. presented a computational study of molybdenum nitride (MoN_2) nanosheets as an electrocatalyst for NH_3 synthesis using DFT.[157] Pure MoN_2 itself is not found to be an ideal catalyst but Fe-doping in MoN_2 can reduce the ΔG_{max} for the rate determining step (RDS) and the so formed Fe-doped MoN_2 can act as a promising catalyst for electrochemical conversion of NH_3 from water and air. Therefore, the untreated MoN_2 can be used as an excellent starting material for designing advanced NRR electrocatalysts.

Sun et al. demonstrated the non-noble metal electrocatalyst Mo_2N nanorods for the first time as an efficient electrocatalyst to convert N_2 to NH_3 under ambient conditions in 0.1 M HCl and achieved a high FE of 4.5% and a NH_3 yield of 78.4 mg h^{-1} mg_{cat}^{-1} at -0.3 V vs. RHE, which is substantially higher than that of a MoO_2 precursor.[158] The DFT calculations revealed that after nitrogenation of MoO_2, the free energy barrier (ΔG_{H^*}) of the potential determining step of NRR decreases dramatically. The same group further synthesised the MoN nanosheet array on the carbon cloth (MoN NA/CC) as an efficient catalyst for NRR with a high NH_3 yield of 3.01×10^{-10} mol s^{-1} cm^{-2} and a FE of 1.15% at -0.3 V vs. RHE in 0.1 M HCl.[159] DFT calculations revealed that MoN NA/CC follow the MvK mechanism for NRR. Further, Wang et al. for the first time modified the MoN electrocatalyst with cation vacancies by fabricating MoN nanocrystals with sufficient Mo vacancies in a N-doped hierarchical porous carbon framework (MV-MoN@NC) because engineering cation vacancy in the TMNs is an effective strategy to improve the electrochemical NRR response.[160] The formation of defects within the sample was proved by X-ray diffraction (XRD) and X-ray photoelectron spectroscopy (XPS) studies. MV-MoN@NC in comparison with non-defective samples MoN, NC, and MoN@NC exhibited best catalytic activity with 76.9 µg h^{-1} mg^{-1} cat. ammonia yield and 6.9% FE at -0.2 V vs. RHE with stability up to 48 h. The cation vacancy decorated MV-MoN@NC has shown a much superior NH_3 production rate to that of reported electrocatalysts with anion vacancies. The occurrence of NRR via MvK was confirmed by the NMR technique which gave the qualitative analysis of the ^{15}N isotopic experiment by weakening of triplet coupling of $^{14}NH_4^+$ in the NMR spectra when ^{15}N is used as a feed gas. The improvement in the NRR activity was confirmed by computational and experimental results, which revealed that Mo vacancies in the MoN surface regulate the electronic structure of MoN and reduce the barrier height from 1.40 to 0.61 eV for the potential-determining step (PDS). Further, local density of states (LDOS) revealed that Mo vacancies created strong hybridisation between molecular orbitals and Mo d orbitals, which led to the easy release of NH_3 molecules as the strength between N and Mo atoms got decreased. This work provides a new pathway of synthesizing electrocatalysts with cation defects in nitrides to catalyze N_2 reduction. Shanmugam et al. recently prepared an efficient and cost-effective electrocatalyst: cubic molybdenum nitride (γ-Mo_2N) nanoparticles by an in situ nitridation method on two-dimensional hexagonal boron nitride (h-BN) sheets.[161] The interfacial engineering of the Mo_2N-BN bridge is found to be selective for N_2 reduction. This way of controlling the

defects to design the electronic structure of the catalyst can be an effective way for selective NRR.

Vacancy creation within the catalyst has great impact on enhancing the intrinsic activity of electrocatalysts because there occurs alteration in the electronic structure, adsorption–desorption energies of the intermediates and surface charge-transfer properties. For example, oxygen vacancies[162] and nitrogen vacancies[121] improved the adsorption and activation of N_2 molecules for subsequent reaction steps. In the case of TMN-based NRR electrocatalysts following the MvK mechanism, N-vacancies have an important role to play. In the MvK mechanism, N-vacancies are created by the release of NH_3 molecules and are replenished with the feed of N_2. There occurs cycling between the empty and filled states. Qiao et al. prepared a 2D layered W_2N_3 nanosheet having N-vacancies.[37] These N-vacancies were characterized by a series of ex situ synchrotron-based EXFAS measurements and were found to be active for NRR with a NH_3 production rate of 11.66 ± 0.98 µg h^{-1} mg_{cat}^{-1} and a FE of 11.67 ± 0.93% at -0.2 V vs. RHE. Further DFT calculations also suggested that N-vacancies on W_2N_3 facilitate N_2 adsorption and also lower the thermodynamic limiting potential for NRR.

Qu et al. developed a VN nanowire array on carbon cloth (VN/CC) via nitridation of the V_2O_5 nanowire array precursor and achieved a high NH_3 yield (2.48×10^{-10} mol^{-1} s^{-1} cm^{-2}) and a FE of 3.58% at -0.3 V vs. RHE in 0.1 M HCl.[163] This work along with providing us an efficient catalyst material for NRR in acidic media also opens up a new avenue for TMNs in NRR.

For mechanistic studies of MvK in NRR, Yan et al. performed quantitative isotope-exchange experiments to determine the density of active sites in the initial and steady state in NRR catalysts (Fig. 9a).[36] In $^{14}N/^{15}N$-exchange experiments, the initial active sites were identified by the amount of $^{14}NH_3$ formed with ^{15}N as a feed. Then, in the steady state the number of active sites could be determined by subjecting the used catalyst for the second round with ^{14}N as a feed. Therefore, only ^{15}N sites will participate in $^{15}NH_3$ production (Fig. 9b and c). Using this approach, the intrinsic activity and quantitative analysis can be achieved. This study opens up a new way for deep understanding of active sites on TMNs for NRR.

Du's group in a recent study did a critical assessment of the electrocatalytic activity of vanadium(III) nitride, niobium(III) nitride, and Nb_4N_5 for NRR.[158] According to the previous theoretical studies, vanadium and niobium nitrides are expected to be catalytically active toward NRR but this study argued that ammonia is produced in nitride catalysts from lattice N but in a non-catalytic process. So, the present study emphasizes the need of reliable testing and analysis techniques for the right assessment of catalytic properties of the materials.

Within the defect engineering, heteroatom dopants are important participants as they can modulate the surface electronic structure and can reduce the overpotential for the electrocatalytic process to fasten up the NRR process.[164] For non-metal heteroatom doping in pristine catalysts, S, O, B and P are selected. However, in the case of TMNs oxygen doping has shown positive effects on NRR.[162,165] Yang's group presented that partially oxidised VN ($VN_{0.7}O_{0.45}$) is an active and stable
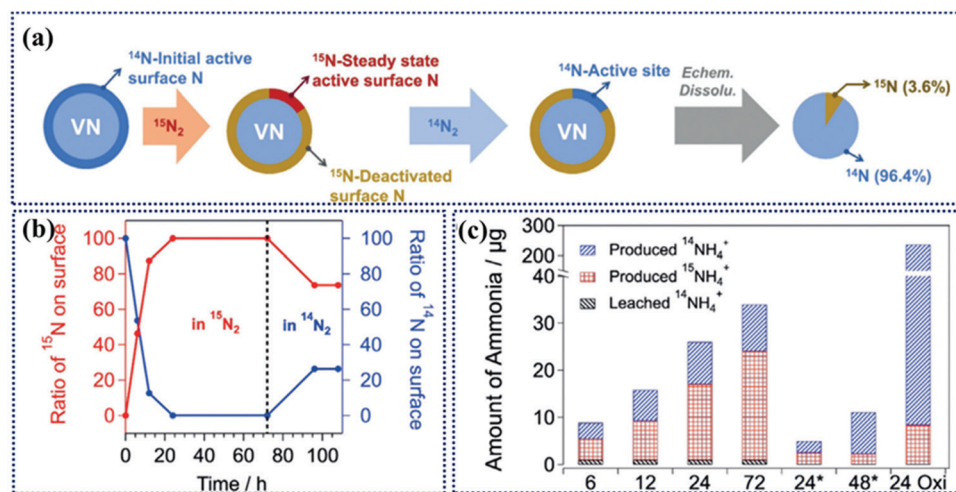
Fig. 9 (a) Schematic illustration representing the isotopic exchange experiments on $V_{14}NO$ to determine the density of active sites of the initial and steady-state in the NRR. (b) Isotopic composition of active surface N sites as a function of time in the NRR. (c) Amounts of $^{14}NH_4^+$ and $^{15}NH_4^+$ produced during the isotopic exchange experiments at various time points during NRR. Reproduced with permission from ref. 36, Copyright 2019, Wiley-VCH Verlag GmbH.

electrocatalyst for NRR that follows the MvK mechanism as confirmed by $^{15}N_2$ experiment.[166]

To study the evolution of the catalyst during the reaction, operando X-ray absorption near edge spectroscopic (XANES) analysis was conducted (Fig. 10a–c). As shown in the figure the

position of the corresponding white lines remains the same with time indicating no detectable leaching of V during NRR. The interesting point is that during NRR there occurs conversion of $VN_{0.7}O_{0.45}$ to VN which is responsible for deactivation of the catalyst. The conversion rate increases as the potential
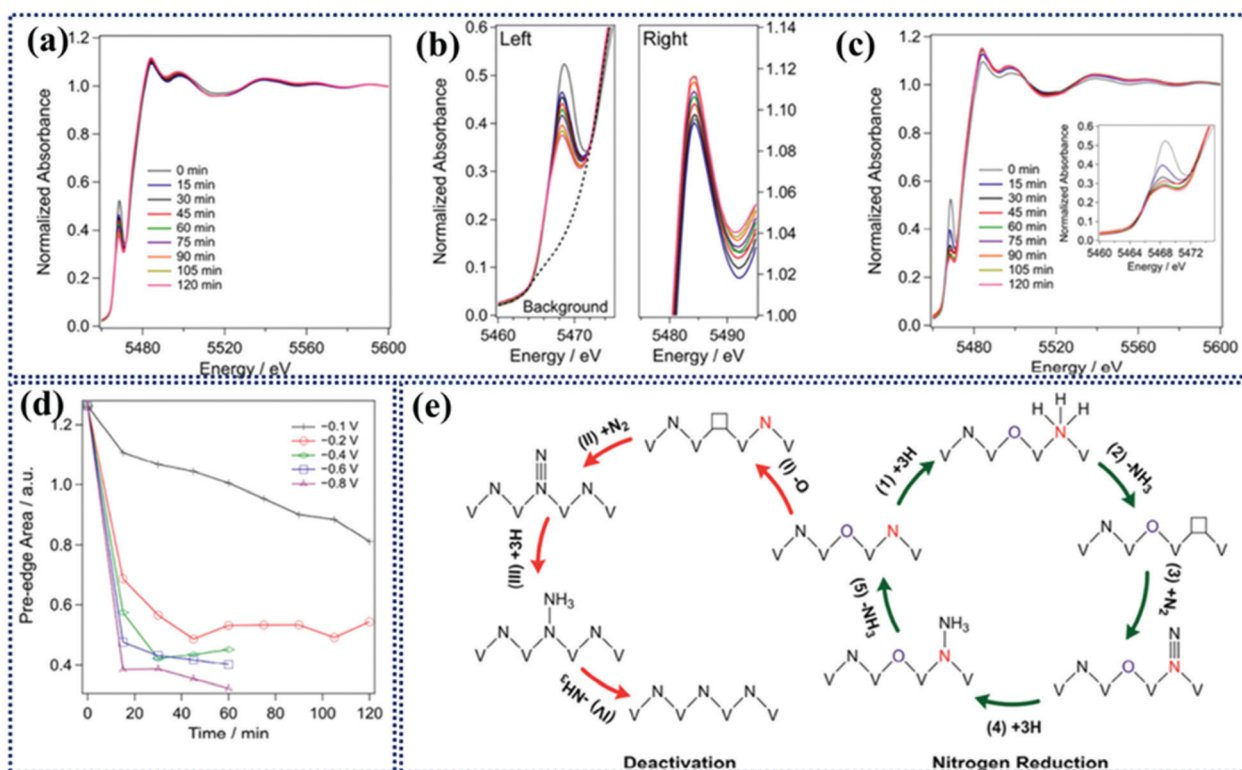
Fig. 10 Operando K-edge XANES spectra of VN at different potentials of (a) 0.1 V and (c) 0.2 V *versus* RHE as a function of time. The inset in (c) shows the corresponding pre-edge peak. (b) The left and right panels show the pre-edge and the white line the peaks at 0.1 V *vs.* RHE as a function of time, respectively. (d) Time-dependent pre-edge area at different potentials. (e) Proposed reaction mechanism for NRR on the surface of $VN_{0.7}O_{0.45}$ *via* the MvK and catalyst deactivation mechanism. Reproduced with permission from ref. 166, Copyright 2018, American Chemical Society.

becomes more negative (Fig. 10d). It is confirmed by the decrease in the intensity of the pre-edge peak. This result was also supported by DFT investigations, that only the N_2 atoms adjacent to surface O are responsible for catalytic activity (Fig. 10e). This work opens up the area for providing more experimental evidence that will verify the hypothesis and the theoretical work.

Another study demonstrating that the performance of TMNs for NRR can be enhanced by partial oxidation was done by Shao et al.[162] Partially oxidized chromium nitride (chromium oxynitride: $CrO_{0.66}N_{0.56}$) nanoparticles were synthesized and their NRR activities were evaluated in a proton exchange membrane electrolyzer (PEMEL) system under ambient conditions. Their NRR activity was found to be better than that of pure Cr_2O_3 and CrN. This finding confirmed the hypothesis that metal oxynitride-based catalysts can act as promising candidates for NRR.

Zhang et al. presented a report with O doping in commercial titanium nitride (TiN) with active phase titanium oxynitride (TiO_xN_y) obtained by plasma etching (PE) of ball-milled TiN.[165] The as-synthesized catalyst TiN-PE with high TiO_xN_y active species delivered a NH_3 yield rate of 3.32×10^{-10} mol s^{-1} cm^{-2} and a FF of 9.1% at -0.6 V vs. RHE in 0.1 M Na_2SO_4 solution which is significantly higher than that achieved for pristine commercial TiN and ball-milled TiN-BM samples. This study gives proof of the benefits of doping for improved catalysis.

Recently, single-atom catalysts (SACs) have gained much attention in the field of catalysis due to their unique electronic structure, uniform distribution of SACs in the substrate and their maximized utilization.[57,167] Many SACs such as Mo,[168] Fe,[169] Sc,[170] Y,[170] Ru,[171] etc. with enhanced NRR activity have been reported. These reported SACs are available in powdered form, so polymer binder is used to attach the catalyst to the current collector that reduces the overall activity of the catalyst. In a recent report, Gao and Zhang developed a 3D-self standing integrated electrode with single Bi atom incorporated hollow titanium nitride (TiN) nanorods encapsulated in a nitrogen-doped carbon layer (NC) supported on carbon cloth (NC/Bi SAs/TiN/CC) for electrocatalytic NRR. The 3D porous structure ensured the maximum exposure of active sites along with efficient mass transfer that improves the catalyst activity. The combined effect of the NC matrix and TiN nanorods prevents the aggregation of Bi SACs and also facilitates the charge transport in NRR. On the other hand, the cooperative effect between Bi SAs and TiN simultaneously promotes the hydrogenation of N_2 and eases the desorption of NH_3. Therefore, NC/Bi SAs/TiN/CC attained a superior FE of 24.60% at -0.5 V vs. RHE and a high NH_3 yield rate of 76.15 µg mg_{cat}^{-1} h^{-1}. This study enforces to work in future on 3D self-supported SACs by rational designing of the structure and electronic configuration for improved catalysis. The TMNs used for NRR have been summarized in Table 3.

7. Conclusion and future perspective

In this work, we have systematically investigated the fundamental practices of the nitrogen reduction process. The kinetics of NRR is governed by a number of factors, which include nitrogen solubility in electrolytes, competitive HER and choice of materials that facilitate NRR over HER. Here for the first time, we have provided a detailed understanding of the solubility of N_2 in different ionic liquid electrolytes, being worked upon to date, which can be further implemented experimentally during NRR. Thereafter, all the factors including choice of electrolyte medium, control of pH and material engineering have been generalized that provide a brief overview of which factors should be kept in mind while performing NRR so that HER could be substantially suppressed. Finally, we have highlighted three categories of catalysts like transition metal borides, carbides and nitrides and discussed their importance in NRR, developments over the ages as well as scopes that could be extended further. These materials could be improvised in a better way considering all the factors and choice of metals highlighted in the review in order to achieve significant NRR in terms of yield, production rate and faradaic efficiency.

● Being an emerging field, there is extensive room for exploration in terms of experimentation in the case of TMBs. The theoretically predicted structures of the TMBs and the presumed conditions of material performance do not often hold true and conventional during their experimental counterpart and naturally discrepancies arise to establish the actual active structure and its mechanistic role in NRR. This would be easier if experiments and theory go hand in hand at this infancy of the TMBs in the field of NRR.

● Recently, mixed metal borides are coming into limelight due to the electronic configuration and orbital overlap between the mixed metals and obviously the synergistic role played by the metals and the boron centre benefitting NRR. Only one

Table 3 A brief summary of TMNs used for NRR

Catalyst	Electrolyte	FE (%)	NH_3 yield rate	Potential	Ref.
MoN NA/CC	0.1 M HCl	1.15	3.01×10^{-10} mol s^{-1} cm^{-2}	-0.3 V vs. RHE	159
W_2N_3	0.1 M KOH	11.67 ± 0.93	11.66 ± 0.98 µg h^{-1} mg_{cat}^{-1}	-0.2 V vs. RHE	37
NC/Bi SAs/TiN/CC	0.1 M Na_2SO_4	24.60 @ -0.5 V vs. RHE	76.15 µg mg_{cat}^{-1} h^{-1} @ -0.8 V RHE	—	188
Mo_2N nanorods	0.1 M HCl	4.5	78.4 µg h^{-1} mg_{cat}^{-1}	-0.3 V vs. RHE	158
VN/CC	0.1 M HCl	3.58	2.48×10^{-10} mol s^{-1} cm^{-2}	-0.3 V vs. RHE	163
VN	0.05 M H_2SO_4	6.0	3.3×10^{-10} mol s^{-1} cm^{-2}	-0.1 V vs. RHE	166
TiN-PE	0.1 M Na_2SO_4	9.1%	3.32×10^{-10} mol s^{-1} cm^{-2}	-0.6 V vs. RHE	165
MV-MoN@NC	0.1 M HCl	6.9%	76.9 µg h^{-1} mg_{cat}^{-1} @ -0.2 V vs. RHE	—	160
$CrO_{0.66}N_{0.56}$		6.9% @ 1.8 V	8.9×10^{-11} mol s^{-1} cm^{-2} @ 2.0 V	—	162

experimental report provides information about mixed metal borides, so there is still a lot of opportunity to tune the choice of metals preferably, which would favour the NRR kinetics.

● Since there are still single reports for several metal borides for NRR, more experimental works and optimizations are desired to verify the reproducibility of the reaction conditions for various metals.

● To leverage high-performance, TMC electrocatalysts are also viable in the upcoming years, the respective major topic areas necessitate a broad focus. Presently, several unique concepts for scalable and reliable fabrication of effectively tailored TMCs need to be suggested for addressing functional electro-catalysts. Integrating numerous modification techniques, notably nanosizing, hybridization, or heteroatom doping, with a convenient fabrication technique throughout one phase or less phases is anticipated.

● Theoretical results might reveal valuable insight regarding the energy transmission pathway of chemical intermediates, which might encourage the development of the desired TMC architecture at the atomic level.

● For further improvement in TMNs as NRR catalysts, the synthesis methods should be understood deeply. Djire *et al.*[172,173] synthesized Ti_2NT_x and $Ti_4N_3T_x$ nitride MXenes and presented their usage in storage and HER. So, nitride MXenes would be an interesting topic to work on their material characterization, MvK mechanism and performance evaluation in NRR.

● *In situ* high-edge experimental tools are required to gain deeper insight into the mechanistic pathways followed by all the categories of catalysts for NRR.

Recently there has been growing interest for the interdisciplinary compounds like TM-boro-carbides and boro-nitrides because of the superconductivity and synergistic effect of the material constituents towards NRR.

Conflicts of interest

There are no conflicts to declare.

Acknowledgements

References

1 D. R. Macfarlane, P. V. Cherepanov, J. Choi, B. H.-R. Suryanto, R. Y. Hodgetts, J. M. Bakker, F. M.-F. Vallana and A. N. Simonov, A Roadmap to the Ammonia Economy., *Joule*, 2020, **4**(6), 1186–1205, DOI: **10.1016/j.joule.2020.04.004**.

2 G. Soloveichik, Electrochemical Synthesis of Ammonia as a Potential Alternative to the Haber–Bosch Process, *Nat.*

Catal., 2019, **2**(5), 377–380, DOI: **10.1038/s41929-019-0280-0**.

3 B. M. Ceballos, G. Pilania, K. P. Ramaiyan, A. Banerjee, C. Kreller and R. Mukundan, Roads Less Traveled: Nitrogen Reduction Reaction Catalyst Design Strategies for Improved Selectivity, *Curr. Opin. Electrochem.*, 2021, **28**, 100723, DOI: **10.1016/j.coelec.2021.100723**.

4 Y. Ren, C. Yu, X. Tan, H. Huang, Q. Wei and J. Qiu, Strategies to Suppress Hydrogen Evolution for Highly Selective Electrocatalytic Nitrogen Reduction: Challenges and Perspectives., *Energy Environ. Sci.*, 2021, **14**(3), 1176–1193, DOI: **10.1039/D0EE03596C**.

5 C. Choi, G. H. Gu, J. Noh, H. S. Park and Y. Jung, Understanding Potential-Dependent Competition between Electrocatalytic Dinitrogen and Proton Reduction Reactions., *Nat. Commun.*, 2021, **12**(1), 4353, DOI: **10.1038/s41467-021-24539-1**.

6 L. Li, C. Tang, D. Yao, Y. Zheng and S. Z. Qiao, Electrochemical Nitrogen Reduction: Identification and Elimination of Contamination in Electrolyte., *ACS Energy Lett.*, 2019, **4**(9), 2111–2116, DOI: **10.1021/ACSENERGYLETT.9B01573**.

7 J. Hou, M. Yang and J. Zhang, Recent Advances in Catalysts, Electrolytes and Electrode Engineering for the Nitrogen Reduction Reaction under Ambient Conditions., *Nanoscale*, 2020, **12**(13), 6900–6920, DOI: **10.1039/D0NR00412J**.

8 D. Ji, T. Li, J. Liu, S. Amirjalayer, M. Zhong, Z.-Y. Zhang, X. Huang, Z. Wei, H. Dong, W. Hu and H. Fuchs, Band-like Transport in Small-Molecule Thin Films toward High Mobility and Ultrahigh Detectivity Phototransistor Arrays., *Nat. Commun.*, 2019, **10**(1), 12, DOI: **10.1038/s41467-018-07943-y**.

9 J. Li, G. Zhan, J. Yang, F. Quan, C. Mao, Y. Liu, B. Wang, F. Lei, L. Li, A. W.-M. Chan, L. Xu, Y. Shi, Y. Du, W. Hao, P. K. Wong, J. Wang, S.-X. Dou, L. Zhang and J. C. Yu, Efficient Ammonia Electrosynthesis from Nitrate on Strained Ruthenium Nanoclusters., *J. Am. Chem. Soc.*, 2020, **142**(15), 7036–7046, DOI: **10.1021/jacs.0c00418**.

10 G.-F. Chen, X. Cao, S. Wu, X. Zeng, L.-X. Ding, M. Zhu and H. Wang, Ammonia Electrosynthesis with High Selectivity under Ambient Conditions *via* a Li+ Incorporation Strategy., *J. Am. Chem. Soc.*, 2017, **139**(29), 9771–9774, DOI: **10.1021/jacs.7b04393**.

11 H. Zhao, D. Zhang, Z. Wang, Y. Han, X. Sun, H. Li, X. Wu, Y. Pan, Y. Qin, S. Lin, Z. Xu, J. Lai and L. Wang, High-Performance Nitrogen Electroreduction at Low Overpotential by Introducing Pb to Pd Nanosponges, *Appl. Catal., B*, 2020, **265**, 118481, DOI: **10.1016/j.apcatb.2019.118481**.

12 X. Chia, P. Lazar, Z. Sofer, J. Luxa and M. Pumera, Layered SnS versus SnS2: Valence and Structural Implications on Electrochemistry and Clean Energy Electrocatalysis., *J. Phys. Chem. C*, 2016, **120**(42), 24098–24111, DOI: **10.1021/acs.jpcc.6b06977**.

13 B. H.-R. Suryanto, D. Wang, L. M. Azofra, M. Harb, L. Cavallo, R. Jalili, D. R.-G. Mitchell, M. Chatti and D. R. MacFarlane, MoS2 Polymorphic Engineering Enhances Selectivity in the Electrochemical Reduction of

Nitrogen to Ammonia., *ACS Energy Lett.*, 2019, **4**(2), 430–435, DOI: **10.1021/acsenergylett.8b02257**.

14 K. Chu, Y. Liu, Y. Li, J. Wang and H. Zhang, Electronically Coupled SnO2 Quantum Dots and Graphene for Efficient Nitrogen Reduction Reaction., *ACS Appl. Mater. Interfaces*, 2019, **11**(35), 31806–31815, DOI: **10.1021/acsami.9b08055**.

15 S. Zhou, X. Yang, W. Pei, Z. Jiang and J. Zhao, MXene and MBene as Efficient Catalysts for Energy Conversion: Roles of Surface, Edge and Interface., *J. Phys. Energy*, 2020, **3**(1), 12002, DOI: **10.1088/2515-7655/abb6d1**.

16 C. N.-R. Rao and G. Ranga Rao, Nature of Nitrogen Adsorbed on Transition Metal Surfaces as Revealed by Electron Spectroscopy and Cognate Techniques., *Surf. Sci. Rep.*, 1991, **13**(7), 223–263, DOI: **10.1016/0167-5729(91)90014-O**.

17 X. Liu, Y. Jiao, Y. Zheng and S.-Z. Qiao, Isolated Boron Sites for Electroreduction of Dinitrogen to Ammonia., *ACS Catal.*, 2020, **10**(3), 1847–1854, DOI: **10.1021/acscatal.9b04103**.

18 Z. Li and Y. Wu, 2D Early Transition Metal Carbides (MXenes) for Catalysis., *Small*, 2019, **15**(29), 1804736, DOI: **10.1002/smll.201804736**.

19 H. Wang, J. Li, K. Li, Y. Lin, J. Chen, L. Gao, V. Nicolosi, X. Xiao and J.-M. Lee, Transition Metal Nitrides for Electrochemical Energy Applications., *Chem. Soc. Rev.*, 2021, **50**(2), 1354–1390, DOI: **10.1039/D0CS00415D**.

20 Z. Qiao, D. Johnson and A. Djire, Challenges and Opportunities for Nitrogen Reduction to Ammonia on Transitional Metal Nitrides *via* Mars-van Krevelen Mechanism, *Cell Rep. Phys. Sci.*, 2021, **2**(5), 100438, DOI: **10.1016/j.xcrp.2021.100438**.

21 A. E. Shilov, Catalytic Reduction of Molecular Nitrogen in Solutions., *Russ. Chem. Bull.*, 2003, **52**(12), 2555–2562, DOI: **10.1023/B:RUCB.0000019873.81002.60**.

22 H.-P. Jia and E. A. Quadrelli, Mechanistic Aspects of Dinitrogen Cleavage and Hydrogenation to Produce Ammonia in Catalysis and Organometallic Chemistry: Relevance of Metal Hydride Bonds and Dihydrogen., *Chem. Soc. Rev.*, 2014, **43**(2), 547–564, DOI: **10.1039/C3CS60206K**.

23 C.-G. Zhan, J. A. Nichols and D. A. Dixon, Ionization Potential, Electron Affinity, Electronegativity, Hardness, and Electron Excitation Energy: Molecular Properties from Density Functional Theory Orbital Energies., *J. Phys. Chem. A*, 2003, **107**(20), 4184–4195, DOI: **10.1021/jp0225774**.

24 G. Jones, T. Bligaard, F. Abild-Pedersen and J. K. Nørskov, Using Scaling Relations to Understand Trends in the Catalytic Activity of Transition Metals., *J. Phys.: Condens. Matter*, 2008, **20**(6), 64239, DOI: **10.1088/0953-8984/20/6/064239**.

25 C. J.-M. van der Ham, M. T.-M. Koper and D. G.-H. Hetterscheid, Challenges in Reduction of Dinitrogen by Proton and Electron Transfer., *Chem. Soc. Rev.*, 2014, **43**(15), 5183–5191, DOI: **10.1039/C4CS00085D**.

26 M.-M. Shi, D. Bao, S.-J. Li, B.-R. Wulan, J.-M. Yan and Q. Jiang, Anchoring PdCu Amorphous Nanocluster on Graphene for Electrochemical Reduction of N2 to NH3 under Ambient Conditions in Aqueous Solution., *Adv.*

Energy Mater., 2018, **8**(21), 1800124, DOI: **10.1002/aenm.201800124**.

27 H. Xie, Q. Geng, X. Zhu, Y. Luo, L. Chang, X. Niu, X. Shi, A. M. Asiri, S. Gao, Z. Wang and X. Sun, PdP2 Nanoparticles–Reduced Graphene Oxide for Electrocatalytic N2 Conversion to NH3 under Ambient Conditions., *J. Mater. Chem. A*, 2019, **7**(43), 24760–24764, DOI: **10.1039/C9TA09910G**.

28 Y. Ying, K. Fan, X. Luo and H. Huang, Predicting Two-Dimensional Pentagonal Transition Metal Monophosphides for Efficient Electrocatalytic Nitrogen Reduction., *J. Mater. Chem. A*, 2019, **7**(18), 11444–11451, DOI: **10.1039/C8TA11605A**.

29 Z. Wang, Y. Li, H. Yu, Y. Xu, H. Xue, X. Li, H. Wang and L. Wang, Ambient Electrochemical Synthesis of Ammonia from Nitrogen and Water Catalyzed by Flower-Like Gold Microstructures., *ChemSusChem*, 2018, **11**(19), 3480–3485, DOI: **10.1002/cssc.201801444**.

30 S. Back and Y. Jung, On the Mechanism of Electrochemical Ammonia Synthesis on the Ru Catalyst., *Phys. Chem. Chem. Phys.*, 2016, **18**(13), 9161–9166, DOI: **10.1039/C5CP07363D**.

31 Y. Liu, X. Zhu, Q. Zhang, T. Tang, Y. Zhang, L. Gu, Y. Li, J. Bao, Z. Dai and J.-S. Hu, Engineering Mo/Mo 2 C/MoC Hetero-Interfaces for Enhanced Electrocatalytic Nitrogen Reduction, *J. Mater. Chem. A*, 2020, **8**, 8920–8926.

32 M. Shi, D. Bao, B. Wulan, Y. Li, Y. Zhang and J. Yan, Au Sub-Nanoclusters on TiO 2 toward Highly Efficient and Selective Electrocatalyst for N 2 Conversion to NH 3 at Ambient Conditions, *Adv. Mater.*, 2017, **29**, 1606550, DOI: **10.1002/adma.201606550**.

33 K. Chu, Y.-P. Liu, Y.-H. Cheng and Q. Li, Synergistic Boron-Dopants and Boron-Induce Oxygen Vacancies in MnO2 Nanosheets to Promote Electrocatalytic Nitrogen Reduction., *J. Mater. Chem A*, 2020, **8**, 5200–5208, DOI: **10.1039/D0TA00220H**.

34 K. Chu, H. Nan, Q. Li, Y. Guo, Y. Tian and W. Liu, Amorphous MoS 3 Enriched with Sulfur Vacancies for Efficient Electrocatalytic Nitrogen Reduction, *J. Energy Chem.*, 2021, **53**, 132–138, DOI: **10.1016/j.jechem.2020.04.074**.

35 C. Lv, Y. Qian, C. Yan, Y. Ding, Y. Liu and G. Y. Chen, Defect Engineering Metal-Free Polymeric Carbon Nitride Electrocatalyst for Effective Nitrogen Fixation under Ambient Conditions, *Angew. Chem., Int. Ed.*, 2018, **57**(32), 10246–10250, DOI: **10.1002/anie.201806386**.

36 X. Yang, S. Kattel, J. Nash, X. Chang, J. H. Lee, Y. Yan, J. G. Chen and B. Xu, Quantification of Active Sites and Elucidation of the Reaction Mechanism of the Electrochemical Nitrogen Reduction Reaction on Vanadium Nitride, *Angew. Chem., Int. Ed.*, 2019, **58**, 13768–13772, DOI: **10.1002/anie.201906449**.

37 H. Jin, L. Li, X. Liu, C. Tang, W. Xu, S. Chen and L. Song, Nitrogen Vacancies on 2D Layered W 2 N 3: A Stable and Efficient Active Site for Nitrogen Reduction Reaction, *Adv. Mater.*, 2019, **31**, 1902709, DOI: **10.1002/adma.201902709**.

38 H. Hosono, M. Kitano, T.-N. Ye, S.-W. Park, Y. Lu, J. Li and M. Sasase, Contribution of Nitrogen Vacancies to Ammonia Synthesis over Metal Nitride Catalysts., *J. Am. Chem. Soc.*, 2020, **142**(33), 14374–14383, DOI: **10.1021/jacs.0c06624**.

39 S. Ji, Z. Wang and J. Zhao, A Boron-Interstitial Doped C 2 N Layer as a Metal-Free Electrocatalyst for N 2 Fi Xation: A Computational Study, *J. Mater. Chem. A*, 2019, **7**, 2392–2399, DOI: **10.1039/c8ta10497b**.

40 Y. Kong, Y. Li, B. Yang and Z. Li, Boron and nitrogen co-doped porous carbon nanofibers as metal-free electrocatalysts for highly efficient ammonia electrosynthesis, *Mater. Chem. A*, 2019, **7**, 26272–26278, DOI: **10.1039/c9ta06076f**.

41 C. Ling, Y. Zhang, Q. Li, X. Bai, L. Shi and J. Wang, New Mechanism for N2 Reduction: The Essential Role of Surface Hydrogenation., *J. Am. Chem. Soc.*, 2019, **141**(45), 18264–18270, DOI: **10.1021/jacs.9b09232**.

42 Y.-C. Hao, Y. Guo, L.-W. Chen, M. Shu, X.-Y. Wang, T.-A. Bu, W.-Y. Gao, N. Zhang, X. Su, X. Feng, J.-W. Zhou, B. Wang, C.-W. Hu, A.-X. Yin, R. Si, Y.-W. Zhang and C.-H. Yan, Promoting Nitrogen Electroreduction to Ammonia with Bismuth Nanocrystals and Potassium Cations in Water, *Nat. Catal.*, 2019, **2**(5), 448–456, DOI: **10.1038/s41929-019-0241-7**.

43 J. Choi, B. H.-R. Suryanto, D. Wang, H.-L. Du, R. Y. Hodgetts, F. M. Ferrero Vallana, D. R. MacFarlane and A. N. Simonov, Identification and Elimination of False Positives in Electrochemical Nitrogen Reduction Studies., *Nat. Commun.*, 2020, **11**(1), 5546, DOI: **10.1038/s41467-020-19130-z**.

44 J. Jacquemin, M. F. Costa Gomes, P. Husson and V. Majer, Solubility of Carbon Dioxide, Ethane, Methane, Oxygen, Nitrogen, Hydrogen, Argon, and Carbon Monoxide in 1-Butyl-3-Methylimidazolium Tetrafluoroborate between Temperatures 283K and 343K and at Pressures Close to Atmospheric., *J. Chem. Thermodyn.*, 2006, **38**(4), 490–502, DOI: **10.1016/j.jct.2005.07.002**.

45 J. Jacquemin, P. Husson, V. Majer and M. F.-C. Gomes, Low-Pressure Solubilities and Thermodynamics of Solvation of Eight Gases in 1-Butyl-3-Methylimidazolium Hexafluorophosphate, *Fluid Phase Equilib.*, 2006, **240**(1), 87–95, DOI: **10.1016/j.fluid.2005.12.003**.

46 D. Almantariotis, S. Stevanovic, O. Fandiño, A. S. Pensado, A. A.-H. Padua, J.-Y. Coxam and M. F. Costa Gomes, Absorption of Carbon Dioxide, Nitrous Oxide, Ethane and Nitrogen by 1-Alkyl-3-Methylimidazolium (Cnmim, *n* = 2,4,6) Tris(Pentafluoroethyl)Trifluorophosphate Ionic Liquids (EFAP)., *J. Phys. Chem. B*, 2012, **116**(26), 7728–7738, DOI: **10.1021/jp304501p**.

47 D. Almantariotis, A. S. Pensado, H. Q.-N. Gunaratne, C. Hardacre, A. A.-H. Pádua, J.-Y. Coxam and M. F. Costa Gomes, Influence of Fluorination on the Solubilities of Carbon Dioxide, Ethane, and Nitrogen in 1-*n*-Fluoro-Alkyl-3-Methylimidazolium Bis(*n*-Fluoroalkylsulfonyl)Amide Ionic Liquids., *J. Phys. Chem. B*, 2017, **121**(2), 426–436, DOI: **10.1021/acs.jpcb.6b10301**.

48 M. F. Costa Gomes and A. A.-H. Pádua, Interactions of Carbon Dioxide with Liquid Fluorocarbons., *J. Phys. Chem. B*, 2003, **107**(50), 14020–14024, DOI: **10.1021/jp0356564**.

49 T. K. Carlisle, J. E. Bara, C. J. Gabriel, R. D. Noble and D. L. Gin, Interpretation of CO2 Solubility and Selectivity in Nitrile-Functionalized Room-Temperature Ionic Liquids Using a Group Contribution Approach., *Ind. Eng. Chem. Res.*, 2008, **47**(18), 7005–7012, DOI: **10.1021/ie8001217**.

50 F. Zhou, L. M. Azofra, M. Ali, M. Kar, A. N. Simonov, C. McDonnell-Worth, C. Sun, X. Zhang and D. R. MacFarlane, Electro-Synthesis of Ammonia from Nitrogen at Ambient Temperature and Pressure in Ionic Liquids., *Energy Environ. Sci.*, 2017, **10**(12), 2516–2520, DOI: **10.1039/C7EE02716H**.

51 C. S.-M. Kang, X. Zhang and D. R. MacFarlane, Synthesis and Physicochemical Properties of Fluorinated Ionic Liquids with High Nitrogen Gas Solubility., *J. Phys. Chem. C*, 2018, **122**(43), 24550–24558, DOI: **10.1021/acs.jpcc.8b07752**.

52 B. Yang, W. Ding, H. Zhang and S. Zhang, Recent Progress on Electrochemical Synthesis of Ammonia from Nitrogen: Strategies to Improve the Catalytic Activity and Selectivity., *Energy Environ. Sci.*, 2021, **14**, 672–687, DOI: **10.1039/D0EE02263B**.

53 L. Shi, Y. Yin, S. Wang and H. Sun, Rational Catalyst Design for N 2 Reduction under Ambient Conditions: Strategies toward Enhanced Conversion E Ffi Ciency., *ACS Catal.*, 2020, **10**, 6870–6899, DOI: **10.1021/acscatal.0c01081**.

54 G. Qing, R. Ghazfar, S. T. Jackowski, F. Habibzadeh, M. M. Ashtiani, C. Chen, M. R. Smith and T. W. Hamann, Recent Advances and Challenges of Electrocatalytic N 2 Reduction to Ammonia., *Chem. Rev.*, 2020, **120**(12), 5437–5516, DOI: **10.1021/acs.chemrev.9b00659**.

55 H. Xu, K. Ithisuphalap, Y. Li, S. Mukherjee, J. Lattimer, G. Soloveichik and G. Wu, Electrochemical Ammonia Synthesis through N2 and H2O under Ambient Conditions: Theory, Practices, and Challenges for Catalysts and Electrolytes., *Nano Energy*, 2020, **69**, 104469, DOI: **10.1016/J.NANOEN.2020.104469**.

56 J. Wang, B. Huang, Y. Ji, M. Sun, T. Wu, R. Yin and X. Zhu, A General Strategy to Glassy M-Te (M = Ru, Rh, Ir) Porous Nanorods for Efficient Electrochemical N 2 Fixation., *Adv. Mater.*, 2020, **32**, 1907112, DOI: **10.1002/adma.201907112**.

57 H. Zhang, G. Liu, L. Shi, J. Ye, H. Zhang, G. Liu, L. Shi and J. Ye, Single-Atom Catalysts: Emerging Multifunctional Materials in Heterogeneous Catalysis., *Adv. Energy Mater.*, 2018, **8**(1), 1701343, DOI: **10.1002/AENM.201701343**.

58 G.-F. Chen, S. Ren, L. Zhang, H. Cheng, Y. Luo, K. Zhu, L.-X. Ding, H. Wang, G. Chen, S. Y. Ren, L. L. Zhang, H. Cheng, Y. R. Luo, K. H. Zhu, L. Ding and H. H. Wang, Advances in Electrocatalytic N2 Reduction—Strategies to Tackle the Selectivity Challenge., *Small Methods*, 2019, **3**(6), 1800337, DOI: **10.1002/SMTD.201800337**.

59 N. Cao and G. Zheng, Aqueous Electrocatalytic N2 Reduction under Ambient Conditions., *Nano Res.*, 2018, **11**(6), 2992–3008, DOI: **10.1007/S12274-018-1987-Y**.

60 S. Chen, S. Perathoner, C. Ampelli, C. Mebrahtu, D. Su and G. Centi, Room-Temperature Electrocatalytic Synthesis of NH3 from H2O and N2 in a Gas–Liquid–Solid Three-Phase Reactor. ACS Sustain., *Chem. Eng.*, 2017, **5**(8), 7393–7400, DOI: **10.1021/ACSSUSCHEMENG.7B01742**.

61 H. Cheng, L. X. Ding, G. F. Chen, L. Zhang, J. Xue and H. Wang, Molybdenum Carbide Nanodots Enable Efficient

Electrocatalytic Nitrogen Fixation under Ambient Conditions., *Adv. Mater.*, 2018, **30**(46), 1803694, DOI: **10.1002/ADMA.201803694**.

62 S. Mukherjee, D. A. Cullen, S. Karakalos, K. Liu, H. Zhang, S. Zhao, H. Xu, K. L. More, G. Wang and G. Wu, Metal-Organic Framework-Derived Nitrogen-Doped Highly Disordered Carbon for Electrochemical Ammonia Synthesis Using N2 and H2O in Alkaline Electrolytes., *Nano Energy*, 2018, **48**(C), 217–226, DOI: **10.1016/J.NANOEN.2018.03.059**.

63 J. Wang, L. Yu, L. Hu, G. Chen, H. Xin and X. Feng, Ambient Ammonia Synthesis *via* Palladium-Catalyzed Electrohydrogenation of Dinitrogen at Low Overpotential., *Nat. Commun.*, 2018, **9**(1), 1–7, DOI: **10.1038/s41467-018-04213-9**.

64 A. R. Singh, B. A. Rohr, J. A. Schwalbe, M. Cargnello, K. Chan, T. F. Jaramillo, I. Chorkendorff and J. K. Nørskov, Electrochemical Ammonia Synthesis - The Selectivity Challenge., *ACS Catal.*, 2017, **7**(1), 706–709, DOI: **10.1021/ACSCATAL.6B03035**.

65 J. Zhang, T. Wang, P. Liu, S. Liu, R. Dong, X. Zhuang, M. Chen and X. Feng, Engineering Water Dissociation Sites in MoS2 Nanosheets for Accelerated Electrocatalytic Hydrogen Production., *Energy Environ. Sci.*, 2016, **9**(9), 2789–2793, DOI: **10.1039/C6EE01786J**.

66 Y. Yu, C. Wang, Y. Yu, Y. Wang and B. Zhang, Promoting Selective Electroreduction of Nitrates to Ammonia over Electron-Deficient Co Modulated by Rectifying Schottky Contacts., *Sci. China: Chem.*, 2020, **63**(10), 1469–1476, DOI: **10.1007/S11426-020-9795-X**.

67 A. R. Singh, B. A. Rohr, J. A. Schwalbe, M. Cargnello, K. Chan, T. F. Jaramillo, I. Chorkendorff and J. K. Nørskov, Electrochemical Ammonia Synthesis—The Selectivity Challenge., *ACS Catal.*, 2017, **7**(1), 706–709, DOI: **10.1021/acscatal.6b03035**.

68 A. Goyal, G. Marcandalli, V. A. Mints and M. T.-M. Koper, Competition between CO2 Reduction and Hydrogen Evolution on a Gold Electrode under Well-Defined Mass Transport Conditions., *J. Am. Chem. Soc.*, 2020, **142**(9), 4154–4161, DOI: **10.1021/jacs.9b10061**.

69 Y. Song, D. Johnson, R. Peng, D. K. Hensley, P. V. Bonnesen, L. Liang, J. Huang, F. Yang, F. Zhang, R. Qiao, A. P. Baddorf, T. J. Tschaplinski, N. L. Engle, M. C. Hatzell, Z. Wu, D. A. Cullen, H. M. Meyer, B. G. Sumpter and A. J. Rondinone, A Physical Catalyst for the Electrolysis of Nitrogen to Ammonia., *Sci. Adv.*, 2018, **4**(4), 1–9, DOI: **10.1126/sciadv.1700336**.

70 X. Zhao, Z. Yang, A. V. Kuklin, G. V. Baryshnikov, H. Ågren, W. Wang, X. Zhou and H. Zhang, Potassium Ions Promote Electrochemical Nitrogen Reduction on Nano-Au Catalysts Triggered by Bifunctional Boron Supramolecular Assembly., *J. Mater. Chem. A*, 2020, **8**(26), 13086–13094, DOI: **10.1039/D0TA04580B**.

71 Y. Ren, C. Yu, X. Han, X. Tan, Q. Wei, W. Li, Y. Han, L. Yang and J. Qiu, Methanol-Mediated Electrosynthesis of Ammonia., *ACS Energy Lett.*, 2021, **6**(11), 3844–3850, DOI: **10.1021/acsenergylett.1c01893**.

72 K. Kim, N. Lee, C.-Y. Yoo, J.-N. Kim, H. C. Yoon and J.-I. Han, Communication—Electrochemical Reduction of Nitrogen to Ammonia in 2-Propanol under Ambient Temperature and Pressure., *J. Electrochem. Soc.*, 2016, **163**, F610–F612, DOI: **10.1149/2.0231607jes**.

73 S. Z. Andersen, M. J. Statt, V. J. Bukas, S. G. Shapel, J. B. Pedersen, K. Krempl, M. Saccoccio, D. Chakraborty, J. Kibsgaard, P. C.-K. Vesborg, J. Nørskov and I. Chorkendorff, Increasing Stability, Efficiency, and Fundamental Understanding of Lithium-Mediated Electrochemical Nitrogen Reduction., *Energy Environ. Sci.*, 2020, **13**(11), 4291–4300, DOI: **10.1039/D0EE02246B**.

74 M. A. Ortuño, O. Hollóczki, B. Kirchner and N. López, Selective Electrochemical Nitrogen Reduction Driven by Hydrogen Bond Interactions at Metal–Ionic Liquid Interfaces., *J. Phys. Chem. Lett.*, 2019, **10**(3), 513–517, DOI: **10.1021/acs.jpclett.8b03409**.

75 H. Zhong, M. Wang, M. Ghorbani-Asl, J. Zhang, K. H. Ly, Z. Liao, G. Chen, Y. Wei, B. P. Biswal, E. Zschech, I. M. Weidinger, A. V. Krasheninnikov, R. Dong and X. Feng, Boosting the Electrocatalytic Conversion of Nitrogen to Ammonia on Metal-Phthalocyanine-Based Two-Dimensional Conjugated Covalent Organic Frameworks., *J. Am. Chem. Soc.*, 2021, **143**(47), 19992–20000, DOI: **10.1021/jacs.1c11158**.

76 D. Wakerley, S. Lamaison, F. Ozanam, N. Menguy, D. Mercier, P. Marcus, M. Fontecave and V. Mougel, Bio-Inspired Hydrophobicity Promotes CO2 Reduction on a Cu Surface., *Nat. Mater.*, 2019, 18, DOI: **10.1038/s41563-019-0445-x**.

77 H. Y.-F. Sim, J. R.-T. Chen, C. S.-L. Koh, H. K. Lee, X. Han, G. C. Phan-Quang, J. Y. Pang, C. L. Lay, S. Pedireddy, I. Y. Phang, E. K.-L. Yeow and X. Y. Ling, ZIF-Induced d-Band Modification in a Bimetallic Nanocatalyst: Achieving Over 44% Efficiency in the Ambient Nitrogen Reduction Reaction., *Angew. Chem., Int. Ed.*, 2020, **59**(39), 16997–17003, DOI: **10.1002/anie.202006071**.

78 L. H. Kwee, K. C.-S. Lin, L. Y. Hong, L. Chong, P. I. Yee, H. Xuemei, T. Chia-Kuang and L. X. Yi, Favoring the Unfavored: Selective Electrochemical Nitrogen Fixation Using a Reticular Chemistry Approach., *Sci. Adv.*, 2022, **4**(3), eaar3208, DOI: **10.1126/sciadv.aar3208**.

79 C. S.-L. Koh, H. K. Lee, H. Y. Fan Sim, X. Han, G. C. Phan-Quang and X. Y. Ling, Turning Water from a Hindrance to the Promotor of Preferential Electrochemical Nitrogen Reduction., *Chem. Mater.*, 2020, **32**(4), 1674–1683, DOI: **10.1021/acs.chemmater.9b05313**.

80 J. Zheng, Y. Lyu, M. Qiao, R. Wang, Y. Zhou, H. Li, C. Chen, Y. Li, H. Zhou, S. P. Jiang and S. Wang, Photoelectrochemical Synthesis of Ammonia on the Aerophilic-Hydrophilic Heterostructure with 37.8% Efficiency., *Chem*, 2019, **5**(3), 617–633, DOI: **10.1016/j.chempr.2018.12.003**.

81 F. Lai, W. Zong, G. He, Y. Xu, H. Huang, B. Weng, D. Rao, J. A. Martens, J. Hofkens, I. P. Parkin and T. Liu, N2 Electroreduction to NH3 by Selenium Vacancy-Rich ReSe2 Catalysis at an Abrupt Interface, *Angew. Chem., Int. Ed.*, 2020, **59**(32), 13320–13327, DOI: **10.1002/anie.202003129**.

82 L. Li, C. Tang, B. Xia, H. Jin, Y. Zheng and S.-Z. Qiao, Two-Dimensional Mosaic Bismuth Nanosheets for Highly Selective Ambient Electrocatalytic Nitrogen Reduction., *ACS*

Catal., 2019, **9**(4), 2902–2908, DOI: **10.1021/acscatal.9b00366**.

83 Y. Wang, M. Shi, D. Bao, F. Meng, Q. Zhang, Y. Zhou, K. Liu, Y. Zhang, J. Wang, Z. Chen, D. Liu, Z. Jiang, M. Luo, L. Gu, Q. Zhang, X. Cao, Y. Yao, M. Shao, Y. Zhang, X.-B. Zhang, J. G. Chen, J. Yan and Q. Jiang, Generating Defect-Rich Bismuth for Enhancing the Rate of Nitrogen Electroreduction to Ammonia, *Angew. Chem., Int. Ed.*, 2019, **58**(28), 9464–9469, DOI: **10.1002/anie.201903969**.

84 X. Guo, J. Gu, S. Lin, S. Zhang, Z. Chen and S. Huang, Tackling the Activity and Selectivity Challenges of Electro-catalysts toward the Nitrogen Reduction Reaction *via* Atomically Dispersed Biatom Catalysts., *J. Am. Chem. Soc.*, 2020, **142**(12), 5709–5721, DOI: **10.1021/jacs.9b13349**.

85 F. Köleli, D. Röpke, R. Aydin and T. Röpke, Investigation of N2-Fixation on Polyaniline Electrodes in Methanol by Elec-trochemical Impedance Spectroscopy., *J. Appl. Electrochem.*, 2011, **41**(4), 405–413, DOI: **10.1007/s10800-010-0250-3**.

86 P. V. Nidheesh, G. Divyapriya, N. Oturan, C. Trellu and M. A. Oturan, Environmental Applications of Boron-Doped Diamond Electrodes: 1. Applications in Water and Waste-water Treatment., *ChemElectroChem*, 2019, **6**(8), 2124–2142, DOI: **10.1002/celc.201801876**.

87 Q. Wang, Y. Lei, D. Wang and Y. Li, Defect Engineering in Earth-Abundant Electrocatalysts for CO2 and N2 Reduction., *Energy Environ. Sci.*, 2019, **12**(6), 1730–1750, DOI: **10.1039/C8EE03781G**.

88 L. Hu, Z. Xing and X. Feng, Understanding the Electrocatalytic Interface for Ambient Ammonia Synthesis., *ACS Energy Lett.*, 2020, 430–436, DOI: **10.1021/ACSENERGYLETT.9B02679**.

89 E. Skúlason, T. Bligaard, S. Gudmundsdóttir, F. Studt, J. Rossmeisl, F. Abild-Pedersen, T. Vegge, H. Jónsson and J. K. Nørskov, A Theoretical Evaluation of Possible Transition Metal Electro-Catalysts for N2 Reduction., *Phys. Chem. Chem. Phys.*, 2011, **14**(3), 1235–1245, DOI: **10.1039/C1CP22271F**.

90 R. Zhang, X. Ren, X. Shi, F. Xie, B. Zheng, X. Guo and X. Sun, Enabling Effective Electrocatalytic N2 Conversion to NH3 by the TiO2 Nanosheets Array under Ambient Conditions., *ACS Appl. Mater. Interfaces*, 2018, **10**(34), 28251–28255, DOI: **10.1021/ACSAMI.8B06647**.

91 Y. Luo, G. F. Chen, L. Ding, X. Chen, L. X. Ding and H. Wang, Efficient Electrocatalytic N2 Fixation with MXene under Ambient Conditions, *Joule*, 2019, **3**(1), 279–289, DOI: **10.1016/J.JOULE.2018.09.011**.

92 H. Xian, Q. Wang, G. Yu, H. Wang, Y. Li, Y. Wang and T. Li, Electrochemical Synthesis of Ammonia by Zirconia-Based Catalysts at Ambient Conditions, *Appl. Catal., A*, 2019, **581**, 116–122, DOI: **10.1016/J.APCATA.2019.05.025**.

93 N. Lazouski, Z. J. Schiffer, K. Williams and K. Manthiram, Understanding Continuous Lithium-Mediated Electroche-mical Nitrogen Reduction., *Joule*, 2019, **3**(4), 1127–1139, DOI: **10.1016/J.JOULE.2019.02.003**.

94 C. J. Bondue, M. Graf, A. Goyal and M. T.-M. Koper, Suppression of Hydrogen Evolution in Acidic Electrolytes by Electrochemical CO2Reduction., *J. Am. Chem. Soc.*, 2021, **143**(1), 279–285, DOI: **10.1021/JACS.0C10397**.

95 S. Carenco, D. Portehault, C. Boissière, N. Mézailles and C. Sanchez, Nanoscaled Metal Borides and Phosphides: Recent Developments and Perspectives., *Chem. Rev.*, 2013, **113**(10), 7981–8065, DOI: **10.1021/cr400020d**.

96 Y. Zhou, F. Che, M. Liu, C. Zou, Z. Liang, P. De Luna, H. Yuan, J. Li, Z. Wang, H. Xie, H. Li, P. Chen, E. Bladt, R. Quintero-Bermudez, T.-K. Sham, S. Bals, J. Hofkens, D. Sinton, G. Chen and E. H. Sargent, Dopant-Induced Electron Localization Drives CO(2) Reduction to C(2) Hydrocarbons., *Nat. Chem.*, 2018, **10**(9), 974–980, DOI: **10.1038/s41557-018-0092-x**.

97 Z. Guo, J. Zhou and Z. Sun, New Two-Dimensional Transition Metal Borides for Li Ion Batteries and Electrocatalysis., *J. Mater. Chem. A*, 2017, **5**(45), 23530–23535, DOI: **10.1039/C7TA08665B**.

98 Y. Li, L. Li, R. Huang and Y. Wen, Computational Screen-ing of MBene Monolayers with High Electrocatalytic Activ-ity for the Nitrogen Reduction Reaction., *Nanoscale*, 2021, **13**(35), 15002–15009, DOI: **10.1039/D1NR04652G**.

99 S. Luo, M. Li, V. Fung, B. G. Sumpter, J. Liu, Z. Wu and K. Page, New Insights into the Bulk and Surface Defect Structures of Ceria Nanocrystals from Neutron Scattering Study., *Chem. Mater.*, 2021, **33**(11), 3959–3970, DOI: **10.1021/acs.chemmater.1c00156**.

100 S. Li, Y. Wang, J. Liang, T. Xu, D. Ma, Q. Liu, T. Li, S. Xu, G. Chen, A. M. Asiri, Y. Luo, Q. Wu and X. Sun, TiB 2 Thin Fi Lm Enabled Ef Fi Cient NH 3 Electrosynthesis at Ambient Conditions, *Mater. Today Phys.*, 2021, **18**, 100396, DOI: **10.1016/j.mtphys.2021.100396**.

101 Y. Fu, P. Richardson, K. Li, H. Yu, B. Yu, S. Donne, E. Kisi and T. Ma, Transition Metal Aluminum Boride as a New Candidate for Ambient-Condition Electrochemical Ammo-nia Synthesis, *Nano-Micro Lett.*, 2020, **12**(1), 1–13, DOI: **10.1007/S40820-020-0400-Z/FIGURES/4**.

102 Y. Cheng, J. Mo, Y. Li, Y. Zhang and Y. Song, A Systematic Computational Investigation of the Water Splitting and N2 Reduction Reaction Performances of Monolayer MBenes., *Phys. Chem. Chem. Phys.*, 2021, **23**(11), 6613–6622, DOI: **10.1039/D0CP06405J**.

103 X. Yang, C. Shang, S. Zhou and J. Zhao, MBenes: Emerging 2D Materials as Efficient Electrocatalysts for the Nitrogen Reduction Reaction., *Nanoscale Horiz.*, 2020, **5**(7), 1106–1115, DOI: **10.1039/D0NH00242A**.

104 K. Chu, W. Gu, Q. Li, Y. Liu, Y. Tian and W. Liu, Amor-phization Activated FeB2 Porous Nanosheets Enable Effi-cient Electrocatalytic N2 Fixation, *J. Energy Chem.*, 2021, **53**, 82–89, DOI: **10.1016/j.jechem.2020.05.009**.

105 J. Liang, H. Li, F. Liu and J. Lu, Layer-Controlled Low-Power Tunneling Transistors Based on SnS Homojunction, *Adv. Theory Simulations*, 2021, **4**(5), 2000290, DOI: **10.1002/adts.202000290**.

106 Q. Li, C. Liu, S. Qiu, F. Zhou, L. He, X. Zhang and C. Sun, Exploration of Iron Borides as Electrochemical Catalysts for the Nitrogen Reduction Reaction., *J. Mater. Chem. A*, 2019, 7(37), 21507–21513, DOI: **10.1039/C9TA04650J**.

107 M. Yao, Z. Shi, P. Zhang, W.-J. Ong, J. Jiang, W.-Y. Ching and N. Li, Density Functional Theory Study of Single Metal

Atoms Embedded into MBene for Electrocatalytic Conversion of N2 to NH3, *ACS Appl. Nano Mater.*, 2020, **3**(10), 9870–9879, DOI: **10.1021/acsanm.0c01922**.

108 L. Ge, W. Xu, C. Chen, C. Tang, L. Xu and Z. Chen, Rational Prediction of Single Metal Atom Supported on Two-Dimensional Metal Diborides for Electrocatalytic N2 Reduction Reaction with Integrated Descriptor., *J. Phys. Chem. Lett.*, 2020, **11**(13), 5241–5247, DOI: **10.1021/acs.jpclett.0c01582**.

109 B. Jiang, H. Song, Y. Kang, S. Wang, Q. Wang, X. Zhou, K. Kani, Y. Guo, J. Ye, H. Li, Y. Sakka, J. Henzie and Y. Yusuke, A Mesoporous Non-Precious Metal Boride System: Synthesis of Mesoporous Cobalt Boride by Strictly Controlled Chemical Reduction., *Chem. Sci.*, 2020, **11**(3), 791–796, DOI: **10.1039/C9SC04498A**.

110 L. Zhang, X. Ji, X. Ren, Y. Ma, X. Shi, Z. Tian, A. M. Asiri, L. Chen, B. Tang and X. Sun, Electrochemical Ammonia Synthesis *via* Nitrogen Reduction Reaction on a MoS2 Catalyst: Theoretical and Experimental Studies., *Adv. Mater.*, 2018, **30**(28), 1800191, DOI: **10.1002/adma.201800191**.

111 X. Li, T. Li, Y. Ma, Q. Wei, W. Qiu, H. Guo, X. Shi, P. Zhang, A. M. Asiri, L. Chen, B. Tang and X. Sun, Boosted Electrocatalytic N2 Reduction to NH3 by Defect-Rich MoS2 Nanoflower., *Adv. Energy Mater.*, 2018, **8**(30), 1801357, DOI: **10.1002/aenm.201801357**.

112 X. Zhao, X. Lan, D. Yu, H. Fu, Z. Liu and T. Mu, Deep Eutectic-Solvothermal Synthesis of Nanostructured Fe3S4 for Electrochemical N2 Fixation under Ambient Conditions., *Chem. Commun.*, 2018, **54**(92), 13010–13013, DOI: **10.1039/C8CC08045C**.

113 H. Cheng, L.-X. Ding, G.-F. Chen, L. Zhang, J. Xue and H. Wang, Molybdenum Carbide Nanodots Enable Efficient Electrocatalytic Nitrogen Fixation under Ambient Conditions., *Adv. Mater.*, 2018, **30**(46), 1803694, DOI: **10.1002/adma.201803694**.

114 X. Ren, J. Zhao, Q. Wei, Y. Ma, H. Guo, Q. Liu, Y. Wang, G. Cui, A. M. Asiri, B. Li, B. Tang and X. Sun, High-Performance N2-to-NH3 Conversion Electrocatalyzed by Mo2C Nanorod., *ACS Cent. Sci.*, 2019, **5**(1), 116–121, DOI: **10.1021/acscentsci.8b00734**.

115 X. Zhu, Z. Liu, Q. Liu, Y. Luo, X. Shi, A. M. Asiri, Y. Wu and X. Sun, Efficient and Durable N2 Reduction Electrocatalysis under Ambient Conditions: β-FeOOH Nanorods as a Non-Noble-Metal Catalyst., *Chem. Commun.*, 2018, **54**(80), 11332–11335, DOI: **10.1039/C8CC06366D**.

116 H. Hirakawa, M. Hashimoto, Y. Shiraishi and T. Hirai, Photocatalytic Conversion of Nitrogen to Ammonia with Water on Surface Oxygen Vacancies of Titanium Dioxide., *J. Am. Chem. Soc.*, 2017, **139**(31), 10929–10936, DOI: **10.1021/jacs.7b06634**.

117 M.-A. Légaré, G. Bélanger-Chabot, R. D. Dewhurst, E. Welz, I. Krummenacher, B. Engels and H. Braunschweig, Nitrogen Fixation and Reduction at Boron., *Science*, 2018, **359**(6378), 896–900, DOI: **10.1126/science.aaq1684**.

118 Q. Gao, W. Zhang, Z. Shi, L. Yang and Y. Tang, Structural Design and Electronic Modulation of Transition-Metal-Carbide Electrocatalysts toward Efficient Hydrogen Evolution., *Adv. Mater.*, 2019, **31**(2), 1802880, DOI: **10.1002/adma.201802880**.

119 H. Xu, J. Wan, H. Zhang, L. Fang, L. Liu, Z. Huang, J. Li, X. Gu and Y. Wang, Hydrogen Evolution Reaction: A New Platinum-Like Efficient Electrocatalyst for Hydrogen Evolution Reaction at All PH: Single-Crystal Metallic Interweaved V8C7 Networks (Adv. Energy Mater. 23/2018), *Adv. Energy Mater.*, 2018, **8**(23), 1870103, DOI: **10.1002/aenm.201870103**.

120 Z. Shi, K. Nie, Z.-J. Shao, B. Gao, H. Lin, H. Zhang, B. Liu, Y. Wang, Y. Zhang, X. Sun, X.-M. Cao, P. Hu, Q. Gao and Y. Tang, Phosphorus-Mo2C@carbon Nanowires toward Efficient Electrochemical Hydrogen Evolution: Composition, Structural and Electronic Regulation., *Energy Environ. Sci.*, 2017, **10**(5), 1262–1271, DOI: **10.1039/C7EE00388A**.

121 C. Lv, Y. Qian, C. Yan, Y. Ding, Y. Liu, G. Chen and G. Yu, Defect Engineering Metal-Free Polymeric Carbon Nitride Electrocatalyst for Effective Nitrogen Fixation under Ambient Conditions, *Angew. Chem., Int. Ed.*, 2018, **57**(32), 10246–10250, DOI: **10.1002/ANIE.201806386**.

122 M. Naguib, O. Mashtalir, J. Carle, V. Presser, J. Lu, L. Hultman, Y. Gogotsi and M. W. Barsoum, Two-Dimensional Transition Metal Carbides., *ACS Nano*, 2012, **6**(2), 1322–1331, DOI: **10.1021/nn204153h**.

123 Y. Liu, T. G. Kelly, J. G. Chen and W. E. Mustain, Metal Carbides as Alternative Electrocatalyst Supports., *ACS Catal.*, 2013, **3**(6), 1184–1194, DOI: **10.1021/cs4001249**.

124 J. Deng, J. A. Iñiguez and C. Liu, Electrocatalytic Nitrogen Reduction at Low Temperature., *Joule*, 2018, **2**(5), 846–856, DOI: **10.1016/j.joule.2018.04.014**.

125 R. Ge, J. Huo, M. Sun, M. Zhu, Y. Li, S. Chou and W. Li, Surface and Interface Engineering: Molybdenum Carbide–Based Nanomaterials for Electrochemical Energy Conversion., *Small*, 2021, **17**(9), 1903380, DOI: **10.1002/smll.201903380**.

126 M. Kuang, W. Huang, C. Hegde, W. Fang, X. Tan, C. Liu, J. Ma and Q. Yan, Interface Engineering in Transition Metal Carbides for Electrocatalytic Hydrogen Generation and Nitrogen Fixation, *Mater. Horizons*, 2020, **7**(1), 32–53, DOI: **10.1039/C9MH01094G**.

127 Q. Li, S. Qiu, L. He, X. Zhang and C. Sun, Impact of H-Termination on the Nitrogen Reduction Reaction of Molybdenum Carbide as an Electrochemical Catalyst., *Phys. Chem. Chem. Phys.*, 2018, **20**(36), 23338–23343, DOI: **10.1039/C8CP04474K**.

128 I. Matanovic and F. H. Garzon, Nitrogen Electroreduction and Hydrogen Evolution on Cubic Molybdenum Carbide: A Density Functional Study., *Phys. Chem. Chem. Phys.*, 2018, **20**(21), 14679–14687, DOI: **10.1039/C8CP01643G**.

129 H. Xu, X. Yin, X. Li, M. Li, S. Liang, L. Zhang and L. Cheng, Lightweight Ti2CTx MXene/Poly(Vinyl Alcohol) Composite Foams for Electromagnetic Wave Shielding with Absorption-Dominated Feature, *ACS Appl. Mater. Interfaces*, 2019, **11**(10), 10198–10207, DOI: **10.1021/acsami.8b21671**.

130 H. Cheng, L. X. Ding, G. F. Chen, L. Zhang, J. Xue and H. Wang, Molybdenum Carbide Nanodots Enable Efficient

Electrocatalytic Nitrogen Fixation under Ambient Conditions., *Adv. Mater.*, 2018, **30**(46), 1803694, DOI: **10.1002/ADMA.201803694**.

131 K. Ba, G. Wang, T. Ye, X. Wang, Y. Sun, H. Liu, A. Hu, Z. Li and Z. Sun, Single Faceted Two-Dimensional Mo2C Electrocatalyst for Highly Efficient Nitrogen Fixation., *ACS Catal.*, 2020, **10**(14), 7864–7870, DOI: **10.1021/acscatal.0c01127**.

132 Z. W. Chen, X. Y. Lang and Q. Jiang, Discovery of Cobweb-like MoC6 and Its Application for Nitrogen Fixation., *J. Mater. Chem. A*, 2018, **6**(20), 9623–9628, DOI: **10.1039/C8TA03481H**.

133 G. Yu, H. Guo, S. Liu, L. Chen, A. A. Alshehri, K. A. Alzahrani, F. Hao and T. Li, Cr3C2 Nanoparticle-Embedded Carbon Nanofiber for Artificial Synthesis of NH3 through N2 Fixation under Ambient Conditions., *ACS Appl. Mater. Interfaces*, 2019, **11**(39), 35764–35769, DOI: **10.1021/acsami.9b12675**.

134 Z. Fang, D. Fernandez, N. Wang, Z. Bai and G. Yu, Mo2C@3D Ultrathin Macroporous Carbon Realizing Efficient and Stable Nitrogen Fixation., *Sci. China: Chem.*, 2020, **63**(11), 1570–1577, DOI: **10.1007/s11426-020-9740-8**.

135 X. Qu, L. Shen, Y. Mao, J. Lin, Y. Li, G. Li, Y. Zhang, Y. Jiang and S. Sun, Facile Preparation of Carbon Shells-Coated O-Doped Molybdenum Carbide Nanoparticles as High Selective Electrocatalysts for Nitrogen Reduction Reaction under Ambient Conditions., *ACS Appl. Mater. Interfaces*, 2019, **11**(35), 31869–31877, DOI: **10.1021/acsami.9b09007**.

136 L. M. Azofra, N. Li, D. R. MacFarlane and C. Sun, Promising Prospects for 2D D2–D4 M3C2 Transition Metal Carbides (MXenes) in N2 Capture and Conversion into Ammonia., *Energy Environ. Sci.*, 2016, **9**(8), 2545–2549, DOI: **10.1039/C6EE01800A**.

137 Y. Luo, G.-F. Chen, L. Ding, X. Chen, L.-X. Ding and H. Wang, Efficient Electrocatalytic N2 Fixation with MXene under Ambient Conditions., *Joule*, 2019, **3**(1), 279–289, DOI: **10.1016/j.joule.2018.09.011**.

138 D. Liu, G. Zhang, Q. Ji, Y. Zhang and J. Li, Synergistic Electrocatalytic Nitrogen Reduction Enabled by Confinement of Nanosized Au Particles onto a Two-Dimensional Ti3C2 Substrate., *ACS Appl. Mater. Interfaces*, 2019, **11**(29), 25758–25765, DOI: **10.1021/ACSAMI.9B02511/ASSET/IMAGES/LARGE/AM-2019-02511X_0005.JPEG**.

139 S. Liu, J. Luo, Y. Xiong, Z. Chen, K. Zhang, G. Rui, L. Wang, G. Hu, J. Jiang and T. Mei, Taming Polysulfides in an Li–S Battery With Low-Temperature One-Step Chemical Synthesis of Titanium Carbide Nanoparticles From Waste PTFE, *Front. Chem.*, 2021, 638557.

140 T. Shang, Z. Lin, C. Qi, X. Liu, P. Li, Y. Tao, Z. Wu, D. Li, P. Simon and Q. Yang, 3D Macroscopic Architectures from Self-Assembled MXene Hydrogels, *Adv. Funct. Mater.*, 2019, **29**, 1903960, DOI: **10.1002/adfm.201903960**.

141 J. Guo and P. Chen, Catalyst: NH 3 as an Energy Carrier, *CHEMPR*, 2017, 3(5), 709–712, DOI: **10.1016/j.chempr.2017.10.004**.

142 Y. Luo, G. Chen, X. Chen, H. Wang, Y. Luo, G. Chen, L. Ding, X. Chen, L. Ding and H. Wang, Efficient Electrocatalytic N 2 Fixation with MXene under Ambient Conditions Efficient Electrocatalytic N 2 Fixation with MXene under Ambient Conditions., *Joule*, 2019, **3**(1), 279–289, DOI: **10.1016/j.joule.2018.09.011**.

143 H. Huang, F. Gong, Y. Wang, H. Wang, X. Wu, W. Lu, R. Zhao, H. Chen, X. Shi, A. M. Asiri, T. Li, Q. Liu and X. Sun, Mn 3 O 4 Nanoparticles @ Reduced Graphene Oxide Composite: An Efficient Electrocatalyst for Artificial N 2 Fixation to NH 3 at Ambient Conditions, *Nano Res.*, 2019, **12**, 1093–1098.

144 J. Sun, W. Kong, Z. Jin, Y. Han, L. Ma, X. Ding, Y. Niu and Y. Xu, Recent Advances of MXene as Promising Catalysts for Electrochemical Nitrogen Reduction Reaction., *Chinese Chem. Lett.*, 2020, **31**(4), 953–960, DOI: **10.1016/j.cclet.2020.01.035**.

145 G. Yu, H. Guo, S. Liu, L. Chen, A. A. Alshehri, K. A. Alzahrani, F. Hao and T. Li, Cr3C2 Nanoparticle-Embedded Carbon Nanofiber for Artificial Synthesis of NH3 through N2 Fixation under Ambient Conditions., *ACS Appl. Mater. Interfaces*, 2019, **11**(39), 35764–35769, DOI: **10.1021/ACSAMI.9B12675**.

146 F. Wang, L. Xia, X. Li, W. Yang, Y. Zhao and J. Mao, Nano-Ferric Oxide Embedded in Graphene Oxide: High-Performance Electrocatalyst for Nitrogen Reduction at Ambient Condition., *Energy Environ. Mater.*, 2021, **4**(1), 88–94, DOI: **10.1002/EEM2.12100**.

147 Q. Qin, Y. Zhao, M. Schmallegger, T. Heil, J. Schmidt, R. Walczak, G. Gescheidt-Demner, H. Jiao and M. Oschatz, Enhanced Electrocatalytic N 2 Reduction *via* Partial Anion Substitution in Titanium Oxide-Carbon Composites., *Angew. Chem., Int. Ed.*, 2019, **58**(37), 13101–13106, DOI: **10.1002/ANIE.201906056**.

148 S. Sultana, S. Mansingh and K. M. Parida, Phosphide Protected FeS 2 Anchored Oxygen Defect Oriented CeO 2 NS Based Ternary Hybrid for Electrocatalytic and Photocatalytic N 2 Reduction to NH 3., *J. Mater. Chem. A*, 2019, **7**(15), 9145–9153, DOI: **10.1039/C8TA11437D**.

149 S. Qi, Y. Fan, L. Zhao, W. Li and M. Zhao, Two-Dimensional Transition Metal Borides as Highly Efficient N2 Fixation Catalysts., *Appl. Surf. Sci.*, 2021, **536**(May 2020), 147742, DOI: **10.1016/j.apsusc.2020.147742**.

150 G. Qing, R. Ghazfar, S. T. Jackowski, F. Habibzadeh, M. M. Ashtiani, C. P. Chen, M. R. Smith and T. W. Hamann, Recent Advances and Challenges of Electrocatalytic N2Reduction to Ammonia., *Chem. Rev.*, 2020, **120**(12), 5437–5516, DOI: **10.1021/ACS.CHEMREV.9B00659**.

151 Y. Roux, C. Duboc and M. Gennari, Molecular Catalysts for N2 Reduction: State of the Art, Mechanism, and Challenges., *ChemPhysChem*, 2017, **18**(19), 2606–2617, DOI: **10.1002/CPHC.201700665**.

152 X. Yang, J. Nash, J. Anibal, M. Dunwell, S. Kattel, E. Stavitski, K. Attenkofer, J. G. Chen, Y. Yan and B. Xu, Mechanistic Insights into Electrochemical Nitrogen Reduction Reaction on Vanadium Nitride Nanoparticles., *J. Am. Chem. Soc.*, 2018, **140**(41), 13387–13391, DOI: **10.1021/JACS.8B08379**.

153 C. D. Zeinalipour-Yazdi, J. S.-J. Hargreaves and C. R.-A. Catlow, Nitrogen Activation in a Mars-van Krevelen Mechanism for

Ammonia Synthesis on Co3Mo3N., *J. Phys. Chem. C*, 2015, **119**(51), 28368–28376, DOI: **10.1021/ACS.JPCC.5B06811**.

154 Y. Abghoui and E. Skúlason, Onset Potentials for Different Reaction Mechanisms of Nitrogen Activation to Ammonia on Transition Metal Nitride Electro-Catalysts, *Catal. Today*, 2017, **286**, 69–77, DOI: **10.1016/j.cattod.2016.11.047**.

155 Y. Abghoui, A. L. Garden, V. F. Hlynsson, S. Björgvinsdóttir, H. Ólafsdóttir and E. Skúlason, Enabling Electrochemical Reduction of Nitrogen to Ammonia at Ambient Conditions through Rational Catalyst Design, *Phys. Chem. Chem. Phys.*, 2015, **17**(7), 4909–4918, DOI: **10.1039/c4cp04838e**.

156 Y. Abghoui and E. Skúlasson, Transition Metal Nitride Catalysts for Electrochemical Reduction of Nitrogen to Ammonia at Ambient Conditions, *Proc. Comput. Sci.*, 2015, **51**(1), 1897–1906, DOI: **10.1016/j.procs.2015.05.433**.

157 Q. Li, L. He, C. Sun and X. Zhang, Computational Study of MoN2 Monolayer as Electrochemical Catalysts for Nitrogen Reduction, *J. Phys. Chem. C*, 2017, **121**(49), 27563–27568, DOI: **10.1021/acs.jpcc.7b10522**.

158 X. Ren, G. Cui, L. Chen, F. Xie, Q. Wei, Z. Tian and X. Sun, Electrochemical N2 Fixation to NH3 under Ambient Conditions: Mo2N Nanorod as a Highly Efficient and Selective Catalyst, *Chem. Commun.*, 2018, **54**(61), 8474–8477, DOI: **10.1039/C8CC03627F**.

159 L. Zhang, X. Ji, X. Ren, Y. Luo, X. Shi, A. M. Asiri, B. Zheng and X. Sun, Efficient Electrochemical N2 Reduction to NH3 on MoN Nanosheets Array under Ambient Conditions. ACS Sustain, *Chem. Eng.*, 2018, **6**(8), 9550–9554, DOI: **10.1021/acssuschemeng.8b01438**.

160 X. Yang, F. Ling, J. Su, X. Zi, H. Zhang, H. Zhang, J. Li, M. Zhou and Y. Wang, Insights into the Role of Cation Vacancy for Significantly Enhanced Electrochemical Nitrogen Reduction, *Appl. Catal., B*, 2020, **264**, 118477, DOI: **10.1016/j.apcatb.2019.118477**.

161 D. K. Yesudoss, G. Lee and S. Shanmugam, Strong Catalyst Support Interactions in Defect-Rich γ-Mo2N Nanoparticles Loaded 2D-h-BN Hybrid for Highly Selective Nitrogen Reduction Reaction, *Appl. Catal., B*, 2021, **287**(November 2020), 119952, DOI: **10.1016/j.apcatb.2021.119952**.

162 Y. Yao, Q. Feng, S. Zhu, J. Li, Y. Yao, Y. Wang, Q. Wang, M. Gu, H. Wang, H. Li, X. Z. Yuan and M. Shao, Chromium Oxynitride Electrocatalysts for Electrochemical Synthesis of Ammonia Under Ambient Conditions, *Small Methods*, 2019, **3**(6), 1–5, DOI: **10.1002/smtd.201800324**.

163 X. Zhang, R. M. Kong, H. Du, L. Xia and F. Qu, Highly Efficient Electrochemical Ammonia Synthesis: Via Nitrogen Reduction Reactions on a VN Nanowire Array under Ambient Conditions, *Chem. Commun.*, 2018, **54**(42), 5323–5325, DOI: **10.1039/c8cc00459e**.

164 J. Xie, J. Zhang, S. Li, F. Grote, X. Zhang, H. Zhang, R. Wang, Y. Lei, B. Pan and Y. Xie, Controllable Disorder Engineering in Oxygen-Incorporated MoS2 Ultrathin Nanosheets for Efficient Hydrogen Evolution, *J. Am. Chem. Soc.*, 2013, **135**(47), 17881–17888, DOI: **10.1021/JA408329Q**.

165 S. Kang, J. Wang, S. Zhang, C. Zhao, G. Wang, W. Cai and H. Zhang, Plasma-Etching Enhanced Titanium Oxynitride Active Phase with High Oxygen Content for Ambient Electrosynthesis of Ammonia, *Electrochem. Commun.*, 2019, **100**(February), 90–95, DOI: **10.1016/j.elecom.2019.01.028**.

166 X. Yang, J. Nash, J. Anibal, M. Dunwell, S. Kattel, K. Attenkofer, J. G. Chen, Y. Yan and B. Xu, Mechanistic Insights into Electrochemical Nitrogen Reduction Reaction on Vanadium Nitride Nanoparticles, *J. Am. Chem. Soc.*, 2018, **140**(41), 13387–13391, DOI: **10.1021/jacs.8b08379**.

167 Y. Peng, B. Lu, S. Chen, Y. Peng, B. Z. Lu and S. W. Chen, Carbon-Supported Single Atom Catalysts for Electrochemical Energy Conversion and Storage, *Adv. Mater.*, 2018, **30**(48), 1801995, DOI: **10.1002/ADMA.201801995**.

168 L. Han, X. Liu, J. Chen, R. Lin, H. Liu, F. Lü, S. Bak, Z. Liang, Z. S. Hunzheng, E. Stavitski, R. R. Adzic, H. L. Xin, J. P. Chen, H. X. Liu, F. Lü, J. Luo, D. LHan, D. QLin, D. Bak, Z. X. Liang, R. R. Adzic, D. ZZhao, D. Stavitski and H. L. Xin, Atomically Dispersed Molybdenum Catalysts for Efficient Ambient Nitrogen Fixation, *Angew. Chem., Int. Ed.*, 2019, **58**(8), 2321–2325, DOI: **10.1002/ANIE.201811728**.

169 S. Zhang, M. Jin, T. Shi, M. Han, Q. Sun, Y. Lin, Z. Ding, L. R. Zheng, G. Wang, Y. Zhang, H. Zhang and H. Zhao, Electrocatalytically Active Fe-(O-C2)4 Single-Atom Sites for Efficient Reduction of Nitrogen to Ammonia, *Angew. Chem., Int. Ed.*, 2020, **59**(32), 13423–13429, DOI: **10.1002/ANIE.202005930**.

170 J. Liu, X. Kong, L. Zheng, X. Guo, X. Liu and J. Shui, Rare Earth Single-Atom Catalysts for Nitrogen and Carbon Dioxide Reduction, *ACS Nano*, 2020, **14**(1), 1093–1101, DOI: **10.1021/ACSNANO.9B08835**.

171 Z. Geng, Y. Liu, X. Kong, P. Li, K. Li, Z. Liu and J. Du, Achieving a Record-High Yield Rate of 120. 9 μ g NH 3 Mg − for N 2 Electrochemical Reduction over Ru Single-Atom Catalysts, *Adv. Mater.*, 2018, **30**, 1803498, DOI: **10.1002/adma.201803498**.

172 A. Djire, H. Zhang, J. Liu, E. M. Miller and N. R. Neale, Electrocatalytic and Optoelectronic Characteristics of the Two- Dimensional Titanium Nitride Ti 4 N 3 T x MXene, *ACS Appl. Mater. Interfaces*, 2019, **11**, 11812–11823, DOI: **10.1021/acsami.9b01150**.

173 A. Djire, A. Bos, J. Liu, H. Zhang, E. M. Miller and N. R. Neale, Pseudocapacitive Storage in Nanolayered Ti2NTx MXene Using Mg-Ion Electrolyte, *ACS Appl. Nano Mater.*, 2019, **2**, 2785–2795, DOI: **10.1021/acsanm.9b00289**.

174 K. Ba, G. Wang, T. Ye, X. Wang, Y. Sun, H. Liu, A. Hu, Z. Li and Z. Sun, Single Faceted Two-Dimensional Mo2C Electrocatalyst for Highly Efficient Nitrogen Fixation, *ACS Catal.*, 2020, **10**(14), 7864–7870, DOI: **10.1021/ACSCATAL.0C01127/SUPPL_FILE/CS0C01127_SI_001.PDF**.

175 Y. Zhang, J. Hu, C. Zhang, A. T.-F. Cheung, Y. Zhang, L. Liu and M. K.-H. Leung, ScienceDirect Mo 2 C Embedded on Nitrogen-Doped Carbon toward Electrocatalytic Nitrogen Reduction to Ammonia under Ambient Conditions, *Int. J. Hydrogen Energy*, 2021, **46**(24), 13011–13019, DOI: **10.1016/j.ijhydene.2021.01.150**.

176 X. Xu, B. Sun, Z. Liang, H. Cui and J. Tian, High-Performance Electrocatalytic Conversion of N2 to NH3

Using 1T-MoS2 Anchored on Ti3C2 MXene under Ambient Conditions, *ACS Appl. Mater. Interfaces*, 2020, **12**, 26060–26067, DOI: **10.1021/acsami.0c06744**.

177 J. Xia, S. Yang, B. Wang, P. Wu, I. Popovs, H. Li, S. Irle, S. Dai and H. Zhu, Nano Energy Boosting Electrosynthesis of Ammonia on Surface-Engineered MXene Ti 3 C 2, *Nano Energy*, 2020, **72**(February), 104681, DOI: **10.1016/j.nanoen.2020.104681**.

178 J. Zhao, L. Zhang, X. Xie, X. Li, Y. Ma, Q. Liu, W. Fang, X. Shi, G. Cui and X. Sun, Ti3C2Tx (T = F, OH) MXene nanosheets: conductive 2D catalysts for ambient electro-hydrogenation of N2 to NH3, *J. Mater. Chem. A*, 2018, **6**, 24031–24035, DOI: **10.1039/c8ta09840a**.

179 Q. Zhu, W. Wang, W. Abbas, R. Naz, J. Gu, Q. Liu, W. Zhang and D. Zhang, Fluorine-Free Ti3C2Tx (T = O, OH) Nanosheets (∼50–100 Nm) for Nitrogen Fixation under Ambient Conditions, *J. Mater. Chem. A*, 2019, **7**, 14462–14465, DOI: **10.1039/c9ta03254a**.

180 J. Zhang, L. Yang, H. Wang, G. Zhu, H. Wen, H. Feng, X. Sun, X. Guan, J. Wen and Y. Yao, In Situ Hydrothermal Growth of TiO2 Nanoparticles on a Conductive Ti3C2Tx MXene Nanosheet: A Synergistically Active Ti-Based Nano-hybrid Electrocatalyst for Enhanced N2 Reduction to NH3 at Ambient Conditions, *Inorg. Chem.*, 2019, **58**, 5414–5418, DOI: **10.1021/acs.inorgchem.9b00606**.

181 Y. Fang, Z. Liu, J. Han, Z. Jin and Y. Han, High-Performance Electrocatalytic Conversion of N 2 to NH 3 Using Oxygen-Vacancy-Rich TiO 2 In Situ Grown on Ti 3 C 2 T x MXene, *Adv. Energy Mater.*, 2019, **9**, 1803406, DOI: **10.1002/aenm.201803406**.

182 A. H. Wei, Q. Jiang, C. Ampelli, S. Chen, S. Perathoner, Y. Liu and G. Centi, Enhancing N2 Fixation Activity by Converting Ti3C2 MXenes Nanosheets to Nanoribbons, *ChemSusChem*, 2020, **13**, 5614–5619, DOI: **10.1002/cssc.202001719**.

183 Z. Jin, C. Liu, Z. Liu, J. Han, Y. Fang, Y. Han, Y. Niu, Y. Wu, C. Sun and Y. Xu, Rational Design of Hydroxyl-Rich Ti 3 C 2 T x MXene Quantum Dots for High-Performance Electro-chemical N 2 Reduction, *Adv. Energy Mater.*, 2020, **10**, 2000797, DOI: **10.1002/aenm.202000797**.

184 J. Xia, H. Guo, G. Yu, Q. Chen, Y. Liu, Q. Liu, Y. Luo and T. Li, 2D Vanadium Carbide (MXene) for Electrochemical Synthesis of Ammonia Under Ambient Conditions, *Catal. Lett.*, 2021, 0123456789, DOI: **10.1007/s10562-021-03589-6**.

185 A. Liu, X. Liang, Q. Yang, X. Ren, M. Gao and Y. Yang, Electrocatalytic Synthesis of Ammonia Using a 2D Ti 3 C 2 MXene Loaded with Copper Nanoparticles, *Chem-PlusChem*, 2021, **86**, 166–170, DOI: **10.1002/cplu.202000702**.

186 Y. Zeng, X. Du, Y. Li, Y. Guo, Y. Xie, J. Huang, G. Rao, T. Lei, C. Gong, X. Wang and B. Sun, Synergistic Perfor-mance of Nitrogen and Sulfur Co-Doped Ti3C2TX for Electrohydrogenation of N2 to NH3, *J. Alloys Compd.*, 2021, **869**, 159335, DOI: **10.1016/j.jallcom.2021.159335**.

187 C. Du, L. Yang, K. Tang, W. Fang, X. Zhao, Q. Liang, X. Liu, H. Yu, W. Qi and Q. Yan, Ni nanoparticles/V4C3Tx MXene heterostructures for electrocatalytic nitrogen fixation, *Mater. Chem. Front.*, 2021, **5**, 2338–2346, DOI: **10.1039/d0qm00898b**.

188 Z. Xi, K. Shi, X. Xu, P. Jing, B. Liu, R. Gao and J. Zhang, Boosting Nitrogen Reduction Reaction *via* Electronic Cou-pling of Atomically Dispersed Bismuth with Titanium Nitride Nanorods, *Adv. Sci.*, 2022, **9**(4), 2104245, DOI: **10.1002/ADVS.202104245**.

189 E. Skúlason, T. Bligaard, S. Gudmundsdóttir, F. Studt, J. Rossmeisl, F. Abild-Pedersen, T. Vegge, H. Jónsson and J. K. Nørskov, A Theoretical Evaluation of Possible Transi-tion Metal Electro-Catalysts for N2 Reduction, *Phys. Chem. Chem. Phys.*, 2012, **14**(3), 1235–1245, DOI: **10.1039/C1CP22271F**.

190 E. Draževič and E. Skúlason, Are There Any Overlooked Catalysts for Electrochemical NH3 Synthesis—New Insights from Analysis of Thermochemical Data, *iScience*, 2020, **23**(12), 101803, DOI: **10.1016/j.isci.2020.101803**.

191 Y. Xiao, C. Shen and T. Long, Theoretical Establishment and Screening of an Efficient Catalyst for N2 Electroreduc-tion on Two-Dimensional Transition-Metal Borides (MBenes), *Chem. Mater.*, 2021, **33**(11), 4023–4034, DOI: **10.1021/acs.chemmater.1c00424**.

192 X. Guo, S. Lin, J. Gu, S. Zhang, Z. Chen and S. Huang, Establishing a Theoretical Landscape for Identifying Basal Plane Active 2D Metal Borides (MBenes) toward Nitrogen Electroreduction, *Adv. Funct. Mater.*, 2021, **31**(6), 2008056, DOI: **10.1002/adfm.202008056**.

193 C. Ling, X. Niu, Q. Li, A. Du and J. Wang, Metal-Free Single Atom Catalyst for N2 Fixation Driven by Visible Light, *J. Am. Chem. Soc.*, 2018, **140**(43), 14161–14168, DOI: **10.1021/jacs.8b07472**.